

Towards alleviating the H_0 and S_8 tensions with Early Dark Energy – Dark Matter drag

Théo Simon,¹ Tal Adi,² José Luis Bernal,³ Ely D. Kovetz,² Vivian Poulin,¹ and Tristan L. Smith⁴

¹*Laboratoire Univers & Particules de Montpellier (LUPM),
CNRS & Université de Montpellier (UMR-5299),*

Place Eugène Bataillon, F-34095 Montpellier Cedex 05, France

²*Physics Department, Ben-Gurion University of the Negev, Beersheba, Israel*

³*Instituto de Física de Cantabria (IFCA), CSIC-Univ. de Cantabria,
Avda. de los Castros s/n, E-39005 Santander, Spain*

⁴*Department of Physics and Astronomy, Swarthmore College, Swarthmore, PA 19081, USA*

Early dark energy, an additional component of dark energy active in the decade of redshift before recombination, has emerged as one of the most effective models at reducing the “ H_0 tension” between direct measurement of the Hubble parameter H_0 in the late-universe and the Λ CDM prediction when calibrated on *Planck*. However, it requires a slight increase in the dark matter density ω_{cdm} and primordial tilt n_s that worsens the “ S_8 tension” between measurements of weak gravitational lensing at low redshifts and the *Planck*/ Λ CDM prediction. Using a phenomenological fluid model, we investigate whether the inclusion of a drag term between dark matter and early dark energy can compensate for the effect of the increase in power at small-scales, such that both H_0 and S_8 tensions are simultaneously alleviated. We find that this works if the drag term is dynamically relevant in the post-recombination universe. However, a drag term active before or just around the time at which the early dark energy contribution to the energy density is maximum is significantly constrained due to its impact on the matter perturbations before recombination, and the subsequent modifications to the cosmic microwave background power spectra.

I. INTRODUCTION

The increasing precision of observations has revealed discrepancies within the concordance Λ -cold-dark-matter (Λ CDM) cosmological model. Indeed, measurements of some parameters (in particular the H_0 and S_8 parameters) take different values for different observables and experiments (see *e.g.*, Ref. [1] for a recent review). Though the possibility of unknown systematic effects explaining these discrepancies is extensively studied (see *e.g.*, [2–5] for discussion), it is possible that these “cosmic tensions” indicate departure from the consensus Λ CDM paradigm, with new dynamical effects sourcing these apparent discrepancies.

On the one hand, early dark energy (EDE), an additional component of dark energy (DE) active in the decade of redshift before recombination [6–9], has emerged as a promising model to explain the “Hubble tension” between direct measurement of the Hubble parameter in the late-universe and the Λ CDM prediction when calibrated on *Planck* (see Refs. [9–11] for reviews of the models which have been proposed to address the Hubble tension). However, as cosmological observations strongly constrain the expansion history at late times (effectively fixing Ω_m), the increase in H_0 necessarily leads to a large increase in $\omega_m \equiv \Omega_m h^2$, where $h = 100H_0 \text{ km/s/Mpc}$. Therefore, the resulting inferred value of S_8 increases as well [12, 13]. While EDE can compensate the effect of ω_{cdm} in the cosmic microwave background (CMB), it has been found that typically in cosmologies where the Hubble tension is resolved (such as with EDE), the S_8 tension can be exacerbated [14, 15].

On the other hand, the S_8 tension is an indication of

a suppression of power at small-scales, which could be independently resolved thanks to some new dark matter (DM) properties, such as decay or interaction with baryons, dark radiation or DE (see *e.g.*, [16–32]), or some non-linear effect [33, 34]. In particular, Refs. [26–32, 35] suggests that a drag between DM and DE can slow down the falling of DM into gravitational potential wells and thereby suppresses the growth of power.

In this paper, we explore whether a similar effect could have occurred in the pre-recombination universe, between an EDE component and dark matter, and investigate if such a model can simultaneously explain the H_0 and S_8 tensions. Other attempts in that direction have been explored in the literature [36–41], where a coupling between scalar-field EDE and dark matter is introduced at the Lagrangian level (see *e.g.*, [42] for a general discussion). However, the difficulty in such approaches is that there is no unique choice of coupling, and the phenomenology may be very different depending on the choice of coupling and scalar field potential. For instance, Refs. [36, 37, 39] conclude that a Yukawa-like coupling would mostly increase S_8 , as it leads to a stronger gravitational constant at early times (see also Ref. [43]).

Rather than focusing on specific models, we explore a phenomenological approach where the drag is introduced at the level of the linearly perturbed Euler equation, enforcing momentum conservation between an EDE fluid and the DM fluid. As such, our goal is to extract general properties that models must fulfill in order to alleviate both tensions, and provide guidelines for model builders. The caveat is that some aspects of the dynamics included in any specific model may be missing from our phenomenological approach. Given the tight constraints

on the properties of dark matter between recombination and today [44], we expect that any additional effects in specific models beyond modifications to the linearly perturbed Euler equation will lead to further constraints implying that this is likely a conservative approach.

Our paper is structured as follows. In Sec. II, we detail our modeling of the DM-EDE drag and describe the impact on the CMB and matter power spectra. In Sec. III, we perform a series of Bayesian analyses in light of up-to-date compilation of cosmological data to assess whether the model can alleviate both tensions, and we conclude in Sec. IV. In addition, in App. A, we discuss a potential theoretical embedding of our phenomenological model and the issues it currently faces, while in App. B we review the EDE model we consider in this work. Finally, in Apps. C and D, we provide additional material from our analyses.

II. A DRAG BETWEEN DM AND EDE

A. Pure momentum transfer model

There are several possible ways to include a drag between DM and DE. A common phenomenological choice is to model it as an exchange of momentum that modifies the Euler equations with a term $\propto (\theta_c - \theta_\phi)$, where θ_X is the velocity perturbation in species X . However, as we now discuss, this simple phenomenological choice does not follow from more detailed models.

If the EDE is modeled as a scalar field, a well-defined way is to introduce a coupling in the scalar field Lagrangian, following *e.g.* Refs. [35, 42]. As discussed in the literature [36–41], the choice of coupling can generally lead to a broad phenomenology. The simplest coupling that leads to a pure momentum transfer model can be described by the Lagrangian (in the formalism of Ref. [42]):

$$\mathcal{L} = \frac{1}{2} \nabla_\mu \phi \nabla^\mu \phi + \beta (u^\mu \nabla_\mu \phi)^2 - V(\phi), \quad (1)$$

where ϕ is a quintessence scalar field, u^μ is the four-velocity of the fluid, $V(\phi)$ is the potential and β is a coupling constant. Such a coupling leaves the DM continuity equation unaffected, but leads to a modified Euler equation for the CDM:

$$\dot{\theta}_{\text{DM}} + \frac{\dot{a}}{a} \theta_{\text{DM}} = -2\beta \frac{\left(\frac{\dot{\phi}_0}{a} + 2\frac{\dot{a}}{a} \frac{\dot{\phi}_0}{a}\right) \phi_1 + \frac{\dot{\phi}_0}{a} \dot{\phi}_1}{a \left(\bar{\rho}_{\text{DM}} - 2\beta \frac{\dot{\phi}_0^2}{a^2}\right)} k^2, \quad (2)$$

where the scalar field ϕ is expressed in terms of a homogeneous contribution ϕ_0 and a linear perturbation ϕ_1 . Let us note that we use *overdot* to denote conformal time derivative. The coupling of Eq. (1) also leads to modified Klein Gordon equations for the scalar field, which are explicitly given in App. A. It is instructive to write the Euler equation for both species in terms of the field fluid quantities (expressed in App. A), and in the limit of

weak momentum coupling (*i.e.*, when $|\beta| \ll 1$). In that case, we find (using the notation of Ref. [45])

$$\begin{aligned} \dot{\theta}_{\text{DM}} &\approx -\frac{\dot{a}}{a} \theta_c - 2\beta \left(\frac{\delta\rho_\phi}{\bar{\rho}_c} k^2 + 3\frac{\dot{a}}{a} \frac{\bar{\rho}_\phi + \bar{P}_\phi}{\bar{\rho}_c} (1 - c_\phi^2) \theta_\phi \right), \\ \dot{\theta}_\phi &\approx 2\frac{\dot{a}}{a} \theta_\phi + \frac{\delta\rho_\phi}{\bar{\rho}_\phi + \bar{P}_\phi} k^2 + 6\beta \frac{\dot{a}}{a} \theta_c, \end{aligned} \quad (3)$$

where $\bar{\rho}_\phi$ and \bar{P}_ϕ are respectively the energy and pressure of the scalar field, and where $\delta\rho_\phi$ and $c_\phi^2 \equiv \dot{\bar{P}}_\phi/\dot{\bar{\rho}}_\phi$ are respectively the scalar field density perturbation and the adiabatic sound speed. One can see that such a theory derived from first principles does not lead to a drag term $\propto (\theta_c - \theta_\phi)$, unless $\delta\rho_\phi$ is negligible, which is only achieved close to the slow-roll limit, when the EDE scalar field behaves like a cosmological constant. This has been studied in Ref. [35] in the context of DM-DE scattering.

However, an EDE field does not always behave like a cosmological constant. In order to see the impact of a minimal change, here we limit the impact of the coupling to a pure drag term between DM and EDE through a phenomenological approach in which we model EDE and DM as fluids. We introduce the drag term directly at the level of the Euler equations, enforcing momentum conservation between the two fluids. Further discussion about this detailed model and how its phenomenology may differ from a pure drag term is presented in App. A.

B. A phenomenological model of DM–EDE drag

To include the drag in the fluid formalism, working in Newtonian gauge, one simply needs to modify the evolution equations for the velocity divergences θ as

$$\begin{aligned} \dot{\theta}_{\text{DM}} &= -\frac{\dot{a}}{a} \theta_{\text{DM}} + k^2 \psi + \Gamma_{\text{DM/EDE}}(a) (\theta_{\text{EDE}} - \theta_{\text{DM}}), \\ \dot{\theta}_{\text{EDE}} &= -(1 - 3c_{s,\text{EDE}}^2) \frac{\dot{a}}{a} \theta_{\text{EDE}} + \frac{k^2 c_{s,\text{EDE}}^2}{(1 + w_{\text{EDE}})} \delta_{\text{EDE}} \\ &\quad + k^2 \psi - \Gamma_{\text{DM/EDE}}(a) R (\theta_{\text{EDE}} - \theta_{\text{DM}}), \end{aligned} \quad (4)$$

where a is the scale factor, ψ is the gravitational potential, $c_{s,\text{DE}} \equiv 1$ is the EDE sound speed, and w_{EDE} is the EDE equation-of-state parameter. The coefficient

$$R = \frac{\bar{\rho}_{\text{DM}}(a)}{(1 + w_{\text{EDE}}) \bar{\rho}_{\text{EDE}}(a)}, \quad (5)$$

where $\bar{\rho}_i$ are the mean proper energy densities of DM and EDE, ensures momentum conservation. Our choice of EDE model, that was introduced elsewhere and is based on the modified axion-like potential [7, 8, 46] is reviewed in App. B. It is chosen because it has been found to be among the most successful EDE models to reduce the Hubble tension [9] and is favored by ACT CMB data [47, 48], although the latest *Planck* data provide tighter constraints [49]. We do not anticipate major changes

in our conclusions with a different fluid model, see *e.g.* Ref. [50, 51].

The question is then how to parameterize the EDE-DM interaction rate $\Gamma_{\text{DM/EDE}}(a)$. We explore three different choices, motivated by testing different functional forms tied to whether the interaction is active *before*, *around* or *after* the moment where EDE component makes its maximum contribution to the total energy density. First, we make use of the parameterization

$$\Gamma_{\text{DM/EDE}}^{\text{local}}(a) = \beta f_{\text{EDE}}(a), \quad (6)$$

which corresponds to an interaction rate that is relevant only when the EDE contribution to the overall energy density is relevant. We will dub this parameterization the “localized” interaction rate, to emphasize that its contribution is localized around the time at which EDE reaches its peak. Second, we study the case of late-time interaction between DM and EDE, where the interaction rate is relevant only when (late) DE starts dominating the energy budget [28, 32, 52]:

$$\Gamma_{\text{DM/EDE}}^{\text{late}}(a) = \frac{a\beta}{\bar{\rho}_{\text{DM}}(a)} \rho_{\text{EDE},0}, \quad (7)$$

where $\rho_{\text{EDE},0}$ (the EDE energy density today) appears explicitly to ensure that $\Gamma_{\text{DM/EDE}}^{\text{late}}(a) \rightarrow 0$ in the absence of EDE. Note that the rate is $\propto a^4$, such that the interaction is *not* active when the EDE component makes its largest contribution. Rather, it becomes relevant at much later time, around the time at which DE becomes relevant [32]. Such a drag may arise naturally from a model in which EDE transitions to late-time dark energy; we leave the exploration of this possibility for future work. At this stage, we simply test whether the early-time energy injection from the EDE component, together with a late-time drag, can help resolving both tensions. Finally, it is also possible that the drag was active in the early universe, and switches off when the EDE contribution decays away. This resembles for instance the scenario of Ref. [53], where an initially relativistic dark radiation (DR) interacts with dark matter, until it decouples from the cosmic bath implying the cessation of the interaction. We consider a similar scenario, where

$$\Gamma_{\text{DM/EDE}}^{\text{early}}(a) = a^{-5} \beta f_{\text{EDE}}(a). \quad (8)$$

Note that the scaling with a is arbitrary in this phenomenological approach, and we set it such that the ratio $\Gamma/(aH)$ is constant during radiation domination, similarly to what happens in the DM-DR scenario of Ref. [53]. We checked that different scaling before or after the transition does not affect our conclusions.

In the end, for each of the three parameterizations, the only additional free parameter of the model compared to standard EDE is β , the overall amplitude of the interaction. We show the redshift dependence of each interaction rate in Fig. 1, using an EDE model given by $f_{\text{EDE}}(z_c) = 0.1$, $\log_{10}(z_c) = -3.8$, $\Theta_i = 2.9$,

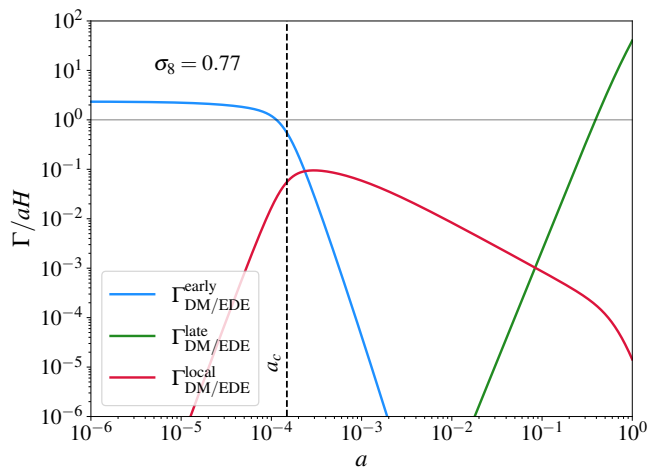


FIG. 1. Scaling of the interaction rate with the scale factor a for the three different parameterizations considered in this work. All three models use the same EDE parameters, and the interaction rates are normalized such that $\sigma_8 \simeq 0.77$.

and values of β that are adjusted such that $\sigma_8 \simeq 0.77$. These correspond approximately to the EDE best-fit parameters extracted from an analysis that combines Planck+BAO+SN1a+ SH_0 ES data (that we will call “ \mathcal{DH} ” in next section), while the values of β are adjusted such that each model approximately give value of S_8 equal to that measured by weak lensing experiments. One can see that, as expected, the early model shows a large interaction rate (namely, $\Gamma > aH$) at $z > z_c$, and quickly drop afterwards. The interaction rate of the local model peaks around z_c , but is quickly negligible before and after z_c . Note that in this case, given the condition of $\sigma_8 \simeq 0.77$, $\Gamma < aH$ at all times. Finally, the interaction rate of the late model increases with a and is only relevant at much later times, closer to dark-energy domination, after which $\Gamma \gg aH$.

C. Impact of EDE-DM drag on the matter and CMB power spectra

We illustrate the effect of the drag term on the matter power spectrum and CMB temperature and polarization anisotropies in Fig. 2 and Fig. 3, respectively, by plotting residuals with respect to Λ CDM. Similarly to Fig. 1, we set EDE and cosmological parameters to the best-fit model of the data combination “ \mathcal{DH} ”, with β adjusted by hand to give $\sigma_8 = 0.77$.

First, in the top panel of Fig. 2, which displays the matter power spectrum residuals at $z = 0$, one can see that the drag between DM and EDE suppresses power on small scales as expected. However, the range of scales affected differs depending on whether the interaction is active prior or after z_c . The “late-time” model has a much stronger effect on the small scales than the “local” and “early-time” models, for which the interactions

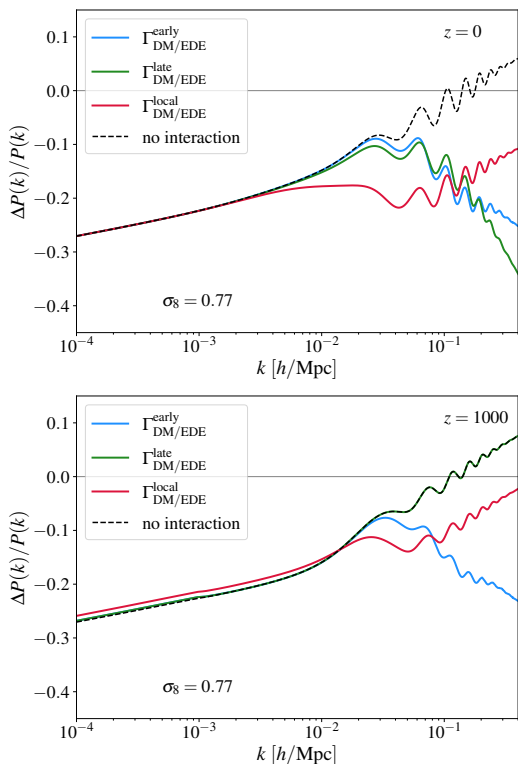


FIG. 2. Residuals of the matter power spectrum between EDE and Λ CDM, with and without the drag term. We illustrate the effect of the three parametrizations of Γ , normalized such that $\sigma_8 \simeq 0.77$.

stop before or around the onset of matter domination. As such, the drag slows down the growth of DM perturbations much more efficiently when it is present at late-times.

Second, the bottom panel of Fig. 2 shows that the late-time drag leaves the matter power spectrum unaffected at $z = 1000$, while the effect of the drag is already imprinted at early times in the other models. Consequently, in Fig. 3, one can see that the “late-time” drag model gives residuals in the CMB TT and EE power spectra that are identical to a model without interaction (black and green lines are super-imposed). On the other hand, a model with drag active around z_c can significantly affect the CMB. Therefore, we anticipate that models with “early-time” or “local” drag will be more easily distinguishable from regular EDE by CMB data than the “late-time” drag model.

III. ANALYSIS

A. Method and data sets

We perform Monte Carlo Markov Chain (MCMC) analyses, confronting the interacting EDE (*i*EDE) models with recent cosmological observations, thanks

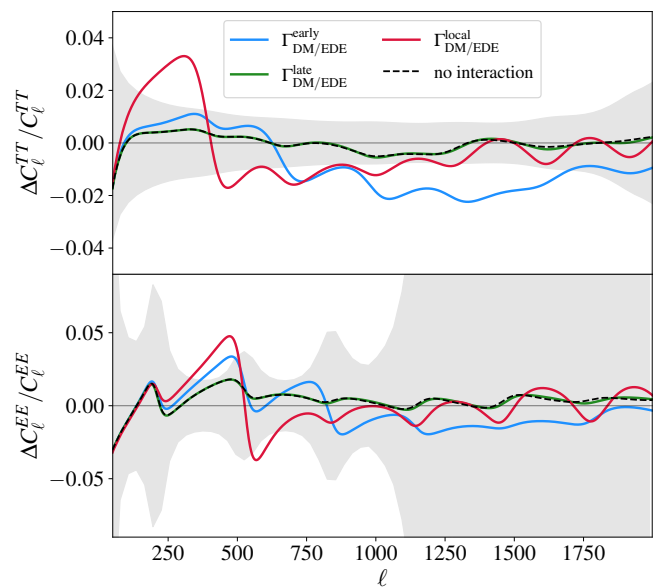


FIG. 3. Residuals of the CMB TT and EE power spectra between EDE and Λ CDM, with and without the drag term. We illustrate the effect of the three parametrizations of Γ , normalized such that $\sigma_8 \simeq 0.77$. The gray bands represent the Planck error bars from the binned PR3 data release.

to the Metropolis-Hastings algorithm from the `MontePython-v3`¹ code [54, 55], which is interfaced with our modified `CLASS` [56, 57] version.² We carry out several analyses using the following datasets:

- **Planck:** The low- ℓ CMB temperature and polarization auto-correlations (TT, EE), and the high- ℓ TT, TE, EE data [58], as well as the gravitational lensing potential reconstruction from *Planck* 2018 [59].
- **ext-BAO:** The low- z BAO data gathered from 6dFGS at $z = 0.106$ [60], SDSS DR7 at $z = 0.15$ [61].
- **EFTofBOSS:** The EFTofLSS analysis of the monopole and quadrupole of the galaxy power spectra from BOSS DR12 luminous red galaxies (LRG), cross-correlated with the reconstructed BAO parameters [62]. The SDSS-III BOSS DR12 galaxy sample data and covariances are described in [63, 64]. The measurements, obtained in [65], are from BOSS catalogs DR12 (v5)³ [66]. They are divided into four skycuts, made up of two redshift bins, namely LOWZ with $0.2 < z < 0.43$ ($z_{\text{eff}} = 0.32$), and CMASS with $0.43 < z < 0.7$ ($z_{\text{eff}} = 0.57$), with north and south galactic skies for each, respectively,

¹ https://github.com/brinckmann/montepython_public

² <https://github.com/PoulinV/AxiCLASS>

³ <https://data.sdss.org/sas/dr12/boos/1ss/>

denoted NGC and SGC. We use the PyBird code⁴ [67] for the theory prediction⁵ as well as for the full-modeling likelihood, together with the “West coast” parametrization (see *e.g.*, Refs [75, 76]).

- **EFTofBOSS:** The EFTofLSS analysis [77] of the monopole and quadrupole of the galaxy power spectra from eBOSS DR16 quasi-stellar objects (QSO) [78]. The QSO catalogs are described in [79] and the covariances are built from the EZ-mocks described in [80]. There are about 343 708 quasars selected in the redshift range $0.8 < z < 2.2$, with $z_{\text{eff}} = 1.52$, divided into two skycuts, NGC and SGC [81, 82]. We also use the PyBird code and the “West coast” parametrization for the eBOSS DR16 full-modeling.
- **Pantheon+:** The Pantheon+ catalog of uncalibrated luminosity distance of type Ia supernovae (SNeIa) in the range $0.01 < z < 2.3$ [83].
- **\mathcal{S} :** Gaussian priors on $S_8 \equiv \sigma_8 \sqrt{\Omega_m}/0.3$ measured by the 3×2 pt weak lensing and galaxy clustering analyses of KiDS-1000+dFLensS+BOSS, $S_8 = 0.766^{+0.020}_{-0.014}$ [84], and DES-Y3, $S_8 = 0.776 \pm 0.017$ [85]. In order to calculate the Gaussian tensions and show the combined constraints on the figures, we use $S_8 = 0.771^{+0.013}_{-0.011}$, which corresponds to the weighted mean and uncertainty of the two priors.⁶
- **\mathcal{H} :** Gaussian prior from the late-time measurement of the absolute calibration of the SNeIa from SH_0ES , $M_b = -19.253 \pm 0.027$ [3], corresponding to $H_0 = (73.04 \pm 1.04)$ km/s/Mpc.

Our baseline dataset, denoted “ \mathcal{D} ”, corresponds to the combination of *Planck*, ext-BAO, EFTofBOSS, EFTofBOSS and Pantheon+ data. We call “ \mathcal{DH} ” the combination of the baseline dataset \mathcal{D} with the SH_0ES prior \mathcal{H} , whereas we denote by “ \mathcal{DS} ” the analyses which consider the combination of the baseline analysis \mathcal{D} with the S_8 priors \mathcal{S} . Finally, the inclusion of all the data is called \mathcal{DHS} .

⁴ <https://github.com/pierrexzy/pybird>

⁵ Strictly speaking, a proper modeling of the late-time drag model would require to modify the EFTofLSS prediction, as the model does not reduce to Λ CDM at late-times. At this stage, we ignore this correction. Note that the BOSS and eBOSS data provide little constraining power in our analysis beyond the BAO measurements that are included in them and that can be applied to models beyond Λ CDM [68], even if it is conceivable that a proper computation of the effect of the drag at late-times would modify these results. We defer this check to future work. In addition, we note that EFTofLSS has already been used in the case of standard EDE in Refs. [69–74].

⁶ We make this choice to emphasize the tension. The combined analysis with “hybrid” pipelines yield $S_8 = 0.790^{+0.018}_{-0.014}$ and would correspondingly reduce the level of detection of the interaction.

For all runs performed, we impose wide uniform priors on the Λ CDM parameters $\{\omega_b, \omega_{\text{cdm}}, H_0, A_s, n_s, \tau_{\text{reio}}\}$, which correspond, respectively, to the dimensionless baryon energy density, the dimensionless CDM energy density, the Hubble parameter today, the variance of curvature perturbations centered around the pivot scale $k_p = 0.05 \text{ Mpc}^{-1}$, the scalar spectral index, and the optical depth to reionization. Regarding the free parameters of the EDE model, we impose a logarithmic prior on z_c and uniform priors on $f_{\text{EDE}}(z_c)$ and Θ_i ,

$$\begin{aligned} 3 &\leq \log_{10}(z_c) \leq 4, \\ 0 &\leq f_{\text{EDE}}(z_c) \leq 0.5, \\ 0 &\leq \Theta_i \leq \pi. \end{aligned}$$

For β , we impose the following logarithmic priors:⁷

$$\begin{aligned} -25 &\leq \log_{10}(\beta^{\text{early}}) \leq -17, \\ -6 &\leq \log_{10}(\beta^{\text{local}}) \leq -1, \\ -11 &\leq \log_{10}(\beta^{\text{late}}) \leq -5. \end{aligned}$$

In this paper, we use the *Planck* neutrino treatment by considering two massless and one massive species with $m_\nu = 0.06 \text{ eV}$ [86]. We consider that our chains have converged when the Gelman-Rubin criterion $R - 1 < 0.05$. Finally, we extract the best-fit parameters from the procedure highlighted in the appendix of Ref. [11], and we acknowledge the use of *GetDist* [87] to extract the probability density functions and produce our plots.

B. Results for all models

In this section, we discuss the ability of the three *i*EDE scenarios to resolve the S_8 tension on top of the H_0 tension. The cosmological constraints of the standard EDE model as well as the three *i*EDE scenarios are displayed in Tabs. I, III and IV for the \mathcal{D} , \mathcal{DH} , \mathcal{DS} and \mathcal{DHS} datasets. In addition, the Q_{DMAP} tensions for S_8 and H_0 , as well as the $\Delta\chi_{\text{min}}^2$ and the associated ΔAIC with respect to Λ CDM, are summarized in Tab. II. In the latter table, we define

$$Q_{\mathcal{DH}}^{H_0} = \sqrt{\chi_{\text{min}}^2(\mathcal{DH}) - \chi_{\text{min}}^2(\mathcal{D})}, \quad (9)$$

$$Q_{\mathcal{DHS}}^{H_0} = \sqrt{\chi_{\text{min}}^2(\mathcal{DHS}) - \chi_{\text{min}}^2(\mathcal{DS})}, \quad (10)$$

as well as

$$Q_{\mathcal{DS}}^{S_8} = \sqrt{\chi_{\text{min}}^2(\mathcal{DS}) - \chi_{\text{min}}^2(\mathcal{D})}, \quad (11)$$

$$Q_{\mathcal{DHS}}^{S_8} = \sqrt{\chi_{\text{min}}^2(\mathcal{DHS}) - \chi_{\text{min}}^2(\mathcal{DH})}. \quad (12)$$

⁷ In practice, for the late model, we effectively run on the combination $\beta\rho_{\text{EDE},0}$ to avoid an explicit dependence on $\rho_{\text{EDE},0}$ in the code. As we never consider explicitly $\rho_{\text{EDE},0} = 0$, it simplifies the parameter space exploration, avoiding complicated degeneracies.

<i>i</i> EDE late				
	\mathcal{D}	\mathcal{DH}	\mathcal{DS}	\mathcal{DHS}
$f_{\text{EDE}}(z_c)$	$< 0.035(0.020)$	$0.066(0.072) \pm 0.014$	$< 0.046(0.032)$	$0.065(0.073) \pm 0.013$
$\log_{10}(z_c)$	$> 3.30(3.95)$	$3.794(3.818)_{-0.088}^{+0.070}$	$> 3.29(3.88)$	$3.778(3.818) \pm 0.076$
Θ_i	unconstrained(3.10)	$> 1.91(2.85)$	unconstrained(3.03)	$> 1.49(2.85)$
$\log_{10}[\Gamma/H_0]$	$< 2.84(0.52)$	$< 2.24(0.74)$	$2.1(1.97)_{-0.68}^{+0.52}$	$1.50(1.51)_{-0.27}^{+0.32}$
H_0	$68.32(68.65)_{-0.77}^{+0.48}$	$71.49(71.80) \pm 0.74$	$68.71(69.31)_{-0.86}^{+0.50}$	$71.48(71.85) \pm 0.70$
ω_{idm}	$0.1215(0.1226)_{-0.0030}^{+0.0014}$	$0.1307(0.1320) \pm 0.0032$	$0.1225(0.1225)_{-0.0032}^{+0.0017}$	$0.1304(0.1321) \pm 0.0029$
$10^2 \omega_b$	$2.245(2.256)_{-0.017}^{+0.015}$	$2.292(2.294) \pm 0.019$	$2.252(2.262)_{-0.019}^{+0.017}$	$2.290(2.295) \pm 0.019$
$10^9 A_s$	$2.112(2.117)_{-0.034}^{+0.030}$	$2.152(2.146) \pm 0.034$	$2.113(2.120)_{-0.033}^{+0.028}$	$2.155(2.150)_{-0.038}^{+0.030}$
n_s	$0.9677(0.9721)_{-0.0060}^{+0.0043}$	$0.9887(0.9914) \pm 0.0059$	$0.9709(0.9760)_{-0.0067}^{+0.0045}$	$0.9884(0.9916) \pm 0.0058$
τ_{reio}	$0.0570(0.0575) \pm 0.0078$	$0.0606(0.0595) \pm 0.0076$	$0.0567(0.0568)_{-0.0075}^{+0.0065}$	$0.0614(0.0602)_{-0.0088}^{+0.0071}$
S_8	$0.800(0.821)_{-0.014}^{+0.022}$	$0.785(0.813)_{-0.018}^{+0.033}$	$0.781(0.779) \pm 0.012$	$0.776(0.777)_{-0.013}^{+0.011}$
Ω_m	$0.3099(0.3094)_{-0.0051}^{+0.0057}$	$0.3018(0.3017)_{-0.0051}^{+0.0045}$	$0.3085(0.3082) \pm 0.0053$	$0.3014(0.3015)_{-0.0053}^{+0.0046}$

TABLE I. Mean (best-fit) $\pm 1\sigma$ (or 2σ for one-sided bounds) of reconstructed parameters of the *i*EDE late model confronted to various datasets.

	EDE				<i>i</i> EDE early				<i>i</i> EDE local				<i>i</i> EDE late			
	\mathcal{D}	\mathcal{DH}	\mathcal{DS}	\mathcal{DHS}	\mathcal{D}	\mathcal{DH}	\mathcal{DS}	\mathcal{DHS}	\mathcal{D}	\mathcal{DH}	\mathcal{DS}	\mathcal{DHS}	\mathcal{D}	\mathcal{DH}	\mathcal{DS}	\mathcal{DHS}
$Q^{H_0} \equiv Q_{\text{DMAP}} \text{ tension } H_0$	3.2σ	–	3.7σ	–	3.3σ	–	3.6σ	–	3.3σ	–	4.2σ	–	3.3σ	–	3.1σ	–
$Q^{S_8} \equiv Q_{\text{DMAP}} \text{ tension } S_8$	3.5σ	3.9σ	–	–	2.9σ	3.3σ	–	–	3.0σ	3.9σ	–	–	1.7σ	1.2σ	–	–
$\Delta\chi^2$	–3.2	–30.1	–0.7	–19.6	–3.3	–30.1	–4.9	–24.4	–3.8	–30.1	–4.9	–19.8	–3.7	–30.3	–10.6	–33.9
ΔAIC	+2.8	–24.1	+5.3	–13.6	+4.7	–22.1	+3.1	–16.4	+4.2	–22.1	+3.1	–11.8	+4.3	–22.3	–2.6	–25.9

TABLE II. Q_{DMAP} tensions, differences in the minimized effective χ^2 , as well as the associated $\Delta\text{AIC} = \Delta\chi^2 + 2 \times \Delta N_p$, where ΔN_p is the difference in the number of free parameters between models, for various combinations of data for the EDE and *i*EDE models.

Finally, in Tab. V of App. D, we show the χ_{min}^2 associated with each likelihood for the different models and combination of datasets considered in this work.

Our main results are summarised in Fig. 4, which shows the 2D posterior distributions reconstructed from the \mathcal{DHS} dataset for the different scenarios studied in this paper. In addition, we display, for the *i*EDE late scenario, the 2D posterior distributions reconstructed from the \mathcal{D} , \mathcal{DH} , \mathcal{DS} and \mathcal{DHS} datasets in Fig. 5, while in App. C we show the same figure for the *i*EDE early and *i*EDE local models. We present here our main results based on these tables and figures:

- Firstly, when S_8 priors are excluded from the analyses, all models lead to a similar alleviation of the H_0 tension with $Q_{\mathcal{DH}}^{H_0} = 3.2 - 3.3\sigma$ (see Tab. II) compared to ΛCDM , where $Q_{\mathcal{DH}}^{H_0} = 6.1\sigma$. This indicates that the presence of the drag does not further help reducing the H_0 tension.
- Secondly, one can see that the discrepancy in S_8 measurements can be alleviated in the *i*EDE late model, with $Q_{\mathcal{DS}}^{S_8} = 1.7\sigma$ and $Q_{\mathcal{DHS}}^{S_8} = 1.2\sigma$. Consequently, one finds a detection of the coupling strength β (as required to lower S_8), with a preference for non-zero β at the 3.8σ level ($\Delta\chi^2 = 14.3$ with respect to EDE, for 1 extra degree of freedom). On the other hand, the early and local *i*EDE models, as well as regular EDE, cannot achieve low- S_8 , with $Q_{\mathcal{DS}}^{S_8} = 2.9 - 3.5\sigma$ and $Q_{\mathcal{DHS}}^{S_8} = 3.3 - 3.9\sigma$.

The early drag model shows a mild level of detection of β with the \mathcal{DS} and \mathcal{DHS} dataset (2σ level), but it is not enough to reduce significantly S_8 . The local model also shows a similar mild preference for non-zero β in the \mathcal{DS} case, but it becomes indistinguishable from regular EDE in the \mathcal{DHS} case (see Fig. 7).

- Finally, the H_0 tension increases for the \mathcal{DHS} dataset (compared to the \mathcal{DH} dataset) for the EDE, *i*EDE early and *i*EDE local models, as a consequence of the fact that a too large H_0 is disfavored when including the low- S_8 priors. However, in the late *i*EDE model, the H_0 tension is slightly lower than previously, with $Q_{\mathcal{DHS}}^{H_0} = 3.1\sigma$.

In conclusion, this confirms the intuition from Sec. II C that the early and local models are more strongly constrained given the impact on the CMB power spectra. This also shows that, while a drag in the DM fluid active at late-times can easily lower S_8 without spoiling the fit to other datasets, the drag cannot occur at the same time as the EDE energy injection. We explore the reasons for those constraints further in the next section.

C. Anatomy of the interactions

In order to understand further why only the late *i*EDE model achieves a reduction of the S_8 and H_0 tensions

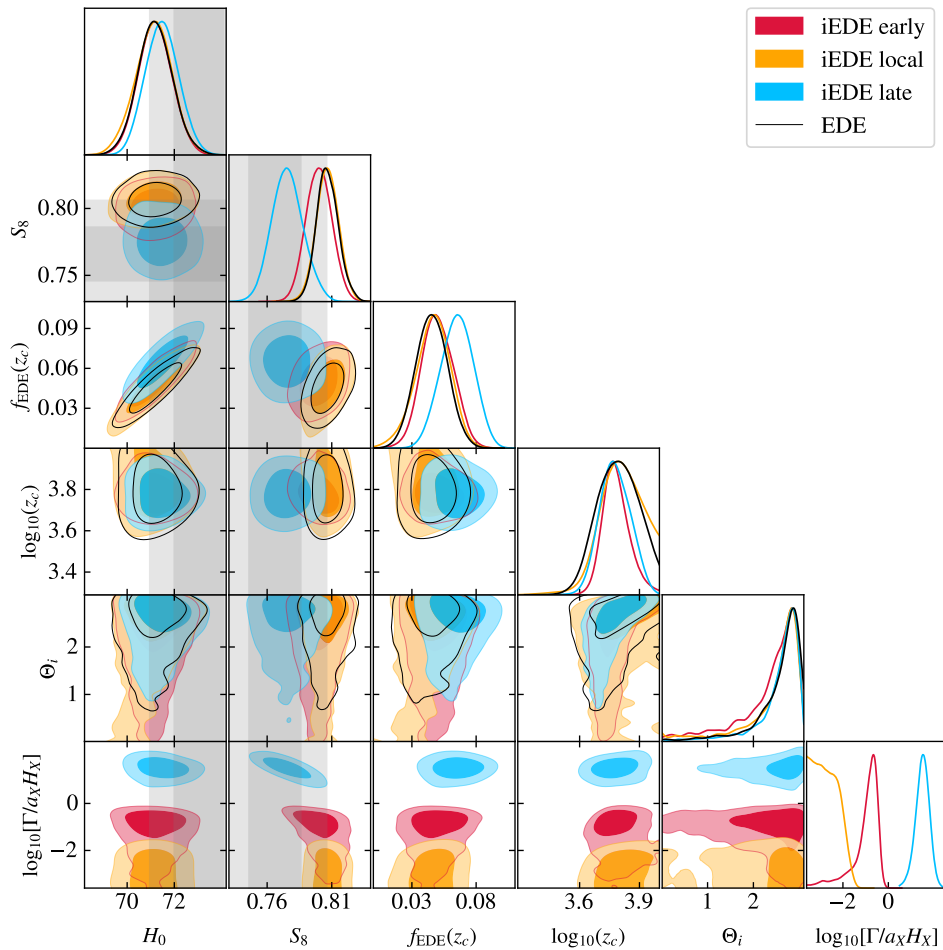


FIG. 4. 2D posterior distributions reconstructed from the \mathcal{DH} dataset for the standard EDE model and the three interacting EDE scenarios. The gray bands show the H_0 and S_8 priors defined in Sec. III. Note that $\log_{10}[\Gamma/a_X H_X]$ is evaluated at $a_X = a_c$ for the early and local interaction scenarios and is evaluated at $a_X = a_0$ for the late interaction scenario.

simultaneously, we compare results of the \mathcal{DS} and \mathcal{DH} analyses in Fig. 5. First and foremost, one can see a clear degeneracy between $\log_{10}[\Gamma/H_0]$ and S_8 in the \mathcal{DH} analysis (dark blue), with a clear overlap of the posteriors with the direct measurements from KiDS and DES (represented in grey). In addition, in the \mathcal{DS} analysis, one can see that the late i EDE model is also favored with respect to both Λ CDM and regular EDE models, with a detection of $\log_{10}[\Gamma/H_0] = 2.1^{+0.52}_{-0.68}$ with $f_{\text{EDE}} < 0.046$. Note that the absence of a lower limit on f_{EDE} in that case is due to the choice of a linear prior on this parameter. Running with a logarithmic prior on f_{EDE} , which emphasizes small values of this parameter, provides a detection of f_{EDE} as shown in the bottom panel of Fig. 6 (see below).

Of particular interest is the plane $\log_{10}(z_c)$ vs S_8 in Fig. 5: it shows that the \mathcal{DS} and \mathcal{DH} datasets prefer the same range of z_c for the EDE to be active. Because the drag is only active at late-times, the degeneracy between f_{EDE} and H_0 that exists for a narrow range of z_c can be

exploited without spoiling the fit. As there is a consistency in the range of z_c favored in both datasets, their combination allows us to resolve both tensions simultaneously.

Comparing with the early and local models of i EDE, shown in Fig. 7 and Fig. 8 of App. C, one can see that the results are very different. In the \mathcal{DS} analysis, only very small fraction of $f_{\text{EDE}}(z_c)$ is allowed. However, we note that a lower S_8 can be reached with a corresponding increase $\log_{10}(z_c)$ compared to the \mathcal{DH} dataset. This suggests that it could be possible to resolve the S_8 tension only at much larger values of z_c and much smaller fraction of $f_{\text{EDE}}(z_c)$ than that favored by the \mathcal{DH} analysis. This indicates that the parameter space region favored in both analyses are mutually inconsistent, and that an EDE-DM drag active prior to recombination cannot resolve both tensions.

To confirm this, we present in Fig. 6 the results of analyses of the three i EDE scenarios for the \mathcal{DS} dataset with larger prior on $\log_{10}(z_c)$ and a log-prior on the EDE

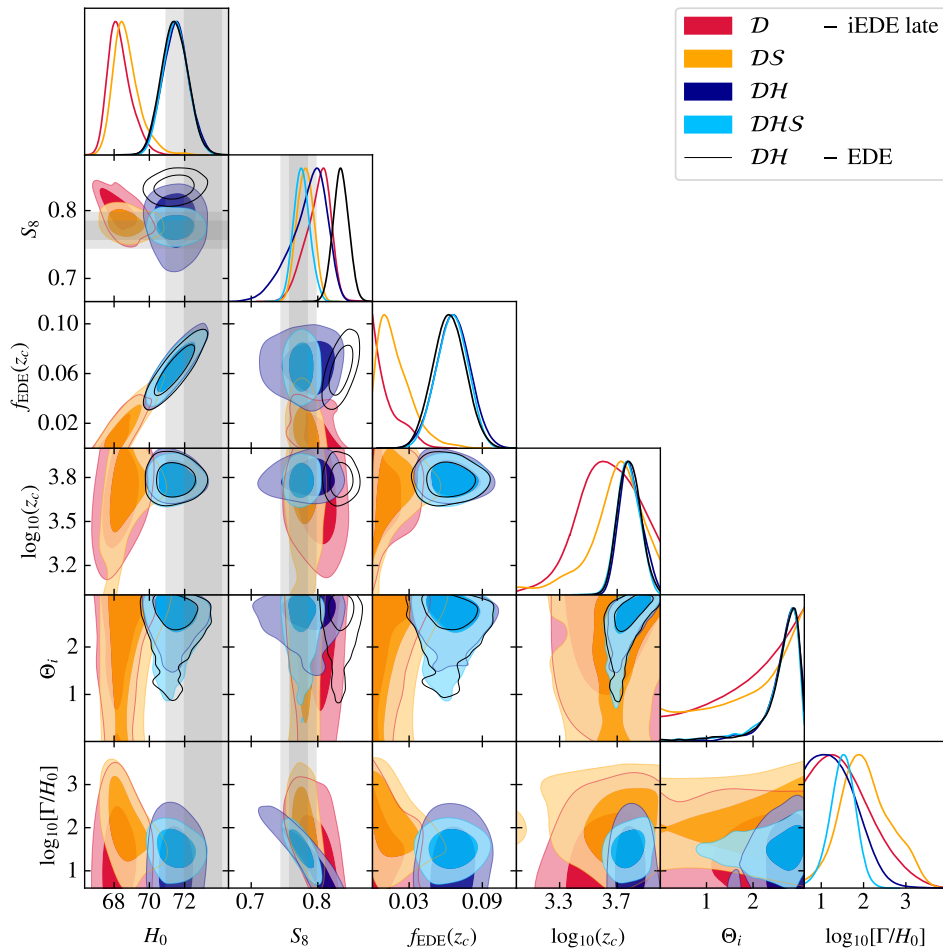


FIG. 5. 2D posterior distributions reconstructed from the D , DH , DS and DHS datasets for the late-interaction EDE scenario. For comparison, we also display the standard EDE 2D posterior distributions reconstructed from the DH dataset. The gray bands show the H_0 and S_8 priors defined in Sec. III.

fraction $f_{\text{EDE}}(z_c)$, to emphasize smaller EDE fractions. Interestingly, in the late iEDE scenario, extending the z_c prior reveals that the data actually favor a drag occurring after the era of recombination ($\log_{10}(z_c) < 3$), which highlights that the drag is preferably not active while the EDE boosts the pre-recombination era expansion rate. In addition, both local and early drag models also manage to lower S_8 for small fraction $f_{\text{EDE}}(z_c) \sim 10^{-4} - 10^{-2}$, as expected. Although the EDE contributes before recombination, for such small fraction, the impact on the sound horizon and H_0 is negligible. One cannot find a simultaneous solution to both tensions in those models, confirming the results with a linear prior on $f_{\text{EDE}}(z_c)$.

IV. CONCLUSIONS

The origin of cosmic tensions in recent years remains an open question extensively explored. In fact, explaining simultaneously the H_0 and S_8 tensions has proven

challenging because, at face value, the SH_0ES calibration of the cosmic distance ladder implies a larger ω_{cdm} , which in turn leads to an earlier matter domination and a larger S_8 [12, 13]. Hence, models that can explain the H_0 tension, such as the EDE models, typically lead to an increase in the S_8 tension. However, it has been shown that the inclusion of a drag term in the DM Euler equation can reduce S_8 , as is done for instance in models of DM-DR interactions, or models of (late-time) DE-DM drag. In this paper, we have investigated whether a drag with DM induced by an EDE component can simultaneously alleviate the H_0 and S_8 tensions.

Building upon the axion-like EDE model, we have introduced a phenomenological drag model between EDE and DM with three different parametrizations of the drag rate, based solely on ensuring energy-momentum conservation, providing thereby flexibility in the modelling. We have paid particular attention to identifying *when* the drag can be introduced in an optimal way. Our results can be summarized as follows:

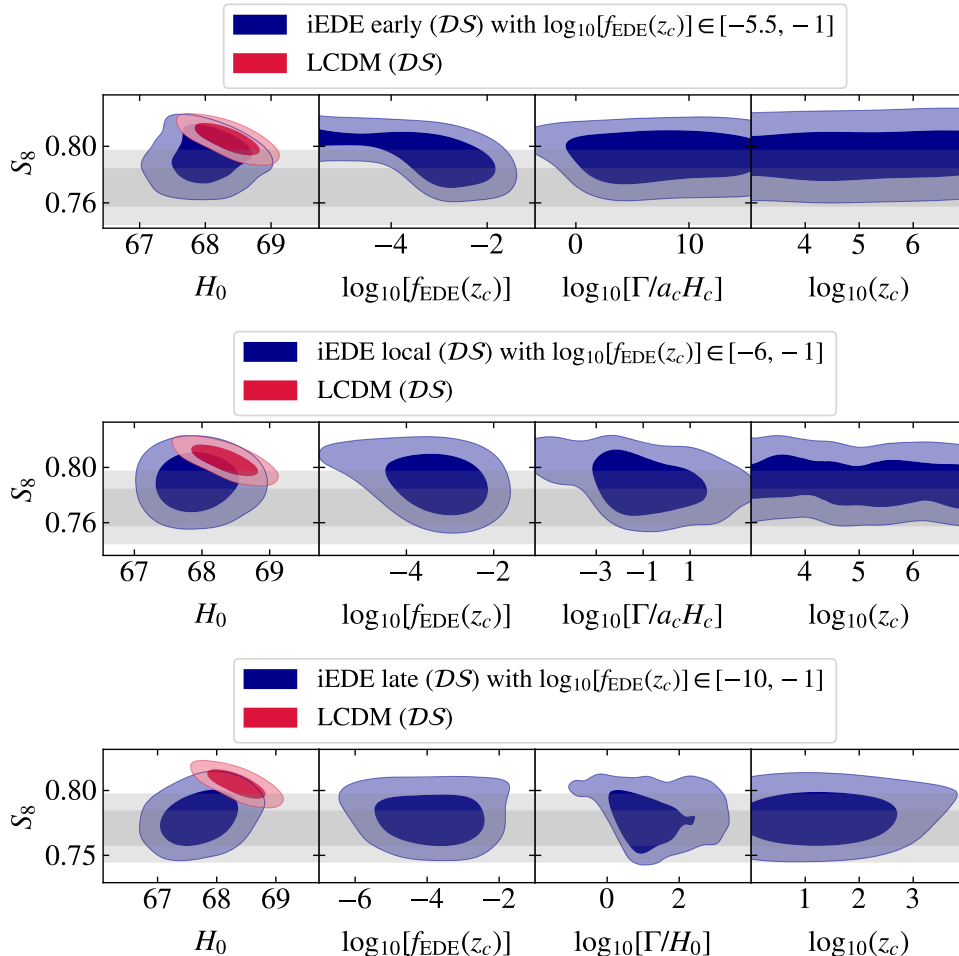


FIG. 6. 2D posterior distributions reconstructed from the DS dataset for the early, local, and late iEDE scenarios with a logarithmic prior on f_{EDE} . For comparison, we also display the ΛCDM constraints on $\{H_0, S_8\}$, while the gray bands show the S_8 priors defined in Sec. III. In the early analysis (*top panel*), we vary $\log_{10} \beta \in [-25, -13]$ and $\log_{10} z_c \in [3, 7]$, in the local analysis (*middle panel*), we vary $\log_{10} \beta \in [-8, 3]$ and $\log_{10} z_c \in [3, 7]$, and in the late analysis (*bottom panel*), we vary $\log_{10} \beta \in [-20, -5]$ and $\log_{10} z_c \in [0, 7]$.

- We have found that only the “late” drag model (where the drag is relevant post-recombination) allows a simultaneous alleviation of the H_0 and S_8 tensions, with a preference for a non-zero drag at the 3.8σ level and no residual S_8 tension.
- The “early” drag model (where the drag is relevant at all times until z_c) shows a 2σ preference for a drag when the S_8 prior is included (DS and DHS analyses), but the S_8 tension remains at the 2.9σ level.
- The “local” drag model (where the drag is relevant only around z_c) is also mildly favored over regular EDE in the DS analysis but cannot alleviate the H_0 and S_8 simultaneously.
- All models yield a similar level of alleviation of the H_0 tension to the $3.2 - 3.3\sigma$ (down from 6.1σ in ΛCDM). The presence of the drag does not further

relax the H_0 tension in a significant way. It only contributes to reducing the S_8 tension.

Our results suggest that the drag cannot be large at the time at which EDE represents a sizeable fraction of the energy density. This is a challenge to this model, given that it appears at face value better motivated for the drag to be important precisely at the time of the EDE energy injection. As we show in App. A, introducing a coupling between a scalar field and dark matter at the Lagrangian level introduces additional effects not captured by our simple parametrization. Our results, while providing a first insight into the exploration of the EDE-DM drag resolution of the cosmic tensions, should thus be understood with some caveats. It will be interesting to extend this work by considering couplings directly at the Lagrangian level in future work to firmly confirm these results.

We note that there are examples of other models which

introduce additional energy density pre-recombination, such as ‘Wess-Zumino dark radiation’, that can both address the Hubble tension and, through a coupling with dark matter, reduce the value of S_8 [53, 88–90]. This highlights the fact that the specific dynamics determine whether a model can address both tensions, motivating a more systematic approach to determine the phenomenological requirements for such models.

ACKNOWLEDGMENTS

The authors acknowledge the use of computational resources from the Excellence Initiative of Aix-Marseille University (A*MIDEX) of the ‘‘Investissements d’Avenir’’ programme. This project has received support from the European Union’s Horizon 2020 research and innovation program under the Marie Skłodowska-Curie grant agreement No 860881-HIDDeN. This project has also received funding from the European Research Council (ERC) under the European Union’s HORIZON-ERC-2022 (Grant agreement No. 101076865). JLB acknowledges funding from the Ramón y Cajal Grant RYC2021-033191-I, financed by MCIN/AEI/10.13039/501100011033 and by the European Union ‘‘NextGenerationEU’’/PRTR, as well as the project UC-LIME (PID2022-140670NA-I00), financed by MCIN/AEI/ 10.13039/501100011033/FEDER, UE. EDK acknowledges joint support from the U.S.-Israel Binational Science Foundation (BSF, grant No. 2022743) and the U.S. National Science Foundation (NSF, grant No. 2307354), as well as support from the ISF-NSFC joint research program (grant No. 3156/23).

Appendix A: A pure moment transfer between scalar field early dark energy and dark matter

Motivating the phenomenological model we outlined above with a theory derived from first principles adds an intriguing aspect to our study. As previously discussed, the simplest coupling can be described by the Lagrangian given by Eq. (1), which we recall here [35, 42]

$$\mathcal{L} = \frac{1}{2} \nabla_\mu \phi \nabla^\mu \phi + \beta (u^\mu \nabla_\mu \phi)^2 - V(\phi), \quad (\text{A1})$$

where ϕ is a quintessence scalar field, u^μ is the four-velocity of the fluid, $V(\phi)$ is the potential, and β is a coupling constant. We limit ourselves to $\beta < 1/2$ to avoid a negative kinetic term. In order to account for the perturbations, we express ϕ in terms of the background and perturbed contributions, $\phi = \phi_0 + \phi_1$. In these terms, the energy density and pressure of the field are [35]

$$\bar{\rho}_\phi = \left(\frac{1}{2} - \beta \right) \frac{\dot{\phi}_0^2}{a^2} + V(\phi), \quad (\text{A2})$$

$$\bar{P}_\phi = \bar{\rho}_\phi - 2V(\phi), \quad (\text{A3})$$

at the background level, and

$$\delta\rho_\phi = (1 - 2\beta) \frac{\dot{\phi}_0 \dot{\phi}_1}{a^2} + V_{,\phi} \phi_1, \quad (\text{A4})$$

$$\delta P_\phi = \delta\rho_\phi - 2V_{,\phi} \phi_1, \quad (\text{A5})$$

at the linearly perturbed level, where subscripts ‘ $,\phi$ ’ refer to derivatives with respect to the scalar field. The equation of motion for the scalar field at the background level is

$$(1 - 2\beta) \left(\ddot{\phi}_0 + 2\frac{\dot{a}}{a} \dot{\phi}_0 \right) + a^2 V_{,\phi} = 0, \quad (\text{A6})$$

while at the perturbed level we have (following the conventions in Ref. [45] for the metric and fluid perturbations in *synchronous* gauge)

$$(1 - 2\beta) \left(\ddot{\phi}_1 + 2\frac{\dot{a}}{a} \dot{\phi}_1 \right) + (k^2 + a^2 V_{,\phi\phi}) \phi_1 + \frac{1}{2} (1 - 2\beta) \dot{\phi}_0 \dot{h} - 2\beta \dot{\phi}_0 \theta_{\text{DM}} = 0, \quad (\text{A7})$$

where h is the trace of the metric perturbations, and

$$\theta_\phi = \frac{1}{1 - 2\beta} \left(k^2 \frac{\phi_1}{\dot{\phi}_0} - 2\beta \theta_{\text{DM}} \right), \quad (\text{A8})$$

is the divergence of the fluid velocity.⁸ The Euler equation for the CDM now reads

$$\dot{\theta}_{\text{DM}} + \frac{\dot{a}}{a} \theta_{\text{DM}} = -2\beta \frac{\left(\frac{\ddot{\phi}_0}{a} + 2\frac{\dot{a}}{a} \frac{\dot{\phi}_0}{a} \right) \varphi_1 + \frac{\dot{\phi}_0}{a} \dot{\phi}_1}{a \left(\bar{\rho}_{\text{DM}} - 2\beta \frac{\dot{\phi}_0^2}{a^2} \right)} k^2. \quad (\text{A9})$$

Writing the Euler equations for both species in terms of the field fluid quantities, we find

$$\dot{\theta}_{\text{DM}} = -\frac{\dot{a}}{a} \theta_{\text{DM}} - G, \quad (\text{A10})$$

$$\dot{\theta}_\phi = 2\frac{\dot{a}}{a} \theta_\phi + \frac{1}{1 - 2\beta} \frac{\delta\rho_\phi}{\bar{\rho}_\phi + \bar{P}_\phi} k^2 + \frac{2\beta}{1 - 2\beta} \left(3\frac{\dot{a}}{a} \theta_{\text{DM}} + G \right),$$

where

$$G \equiv \frac{2\beta}{1 - 2\beta} \frac{\frac{\delta\rho_\phi}{\bar{\rho}_\phi + \bar{P}_\phi} k^2 + 3\frac{\dot{a}}{a} \left(1 - c_\phi^2 \right) [\theta_\phi + 2\beta (\theta_{\text{DM}} - \theta_\phi)]}{\frac{\bar{\rho}_{\text{DM}}}{\bar{\rho}_\phi + \bar{P}_\phi} - \frac{2\beta}{1 - 2\beta}}, \quad (\text{A11})$$

and $c_\phi^2 \equiv \dot{P}_\phi / \dot{\rho}_\phi$ is the adiabatic sound speed. In the limit of weak momentum coupling, $|\beta| \ll 1$, Eq. (A10)

⁸ Note that this convention differs than the one in Refs. [35, 42] by a factor of k^2 .

simplify and now read

$$\begin{aligned}\dot{\theta}_{\text{DM}} &\approx -\frac{\dot{a}}{a}\theta_{\text{DM}} - 2\beta \left(\frac{\delta\rho_\phi}{\bar{\rho}_{\text{DM}}}k^2 + 3\frac{\dot{a}}{a}\frac{\bar{\rho}_\phi + \bar{P}_\phi}{\bar{\rho}_{\text{DM}}} (1 - c_\phi^2)\theta_\phi \right), \\ \dot{\theta}_\phi &\approx 2\frac{\dot{a}}{a}\theta_\phi + \frac{\delta\rho_\phi}{\bar{\rho}_\phi + \bar{P}_\phi}k^2 + 6\beta\frac{\dot{a}}{a}\theta_c.\end{aligned}\quad (\text{A12})$$

While the DM continuity equation is left unaffected, by looking at the full DM evolution in Eq. (A10), or even the weak coupling limit (A12), it is clear that the phenomenological model is missing some of the features of a theory derived from first principles. In addition, the modification to the KG equation suggests that the dynamics of the field can also be affected by this coupling. It will thus be interesting to go beyond the phenomenological approach and test this model explicitly (see *eg*, Ref. [38]), although we expect our approach to lead to conservative constraints as the effect of the coupling is limited to a drag term.

Appendix B: Review of the fluid model of EDE

The fluid EDE model (see Ref. [9]) has an energy density that follows

$$\rho_{\text{EDE}}(a) = \rho_{\text{EDE},0} e^{3 \int_a^1 [1+w_{\text{EDE}}(a)] da/a}, \quad (\text{B1})$$

where $w_{\text{EDE}}(a)$ is the EDE equation of state defined as

$$w_{\text{EDE}}(a) = \frac{1 + w_f}{1 + (a_c/a)^{3(1+w_f)}} - 1, \quad (\text{B2})$$

such that the EDE fluid has $w_{\text{EDE}} \rightarrow -1$ when $a \ll a_c$, and $w_{\text{EDE}} \rightarrow w_f$ when $a \gg a_c$. This parametrization captures the background dynamics of an axion-like scalar field ϕ with a potential $V(\phi) \propto (1 - \cos(\phi/f))^n$ and with a final equation of state $w_f = (n-1)/(n+1)$ [7]. We fix $n = 3$ for simplicity, since data have been shown to be not highly sensitive to this parameter as long as $2 \lesssim n \lesssim 5$. The dynamics of perturbations in the fluid approximation is dictated by the effective sound-speed c_s^2 , that can be approximated, for an oscillating scalar field with a potential ϕ^{2n} , as [7]

$$c_s^2(k, a) = \frac{2a^2(n-1)\varpi^2 + k^2}{2a^2(n+1)\varpi^2 + k^2}, \quad (\text{B3})$$

where ϖ is the angular frequency of the oscillating background field, well-approximated by [8, 46, 91]

$$\begin{aligned}\varpi(a) &\simeq m \frac{\sqrt{\pi}\Gamma(\frac{1+n}{2n})}{\Gamma(1 + \frac{1}{2n})} 2^{-(1+n)/2} \theta_{\text{env}}^{n-1}(a), \\ &\simeq 3H(z_c) \frac{\sqrt{\pi}\Gamma(\frac{1+n}{2n})}{\Gamma(1 + \frac{1}{2n})} 2^{-(1+n)/2} \frac{\theta_{\text{env}}^{n-1}(a)}{\sqrt{|E_{n,\theta\theta}(\theta_i)|}}.\end{aligned}\quad (\text{B4})$$

In this equation, we have written the scalar field potential as $V_n(\phi) = m^2 f^2 E_n(\theta = \phi/f)$, where m and f are respectively the axion mass and decay constant. In addition, $\Gamma(x)$ is the Euler Gamma function corresponding to the envelope of the background field once it is oscillating, $\theta_{\text{env}} \equiv \phi_{\text{env}}/f$, where

$$\phi_{\text{env}}(a) = \phi_c \left(\frac{a_c}{a} \right)^{3/(n+1)}. \quad (\text{B5})$$

As usual for the axion-like EDE model, $f_{\text{EDE}}(z_c)$, $\log_{10}(z_c)$ and Θ_i the three free parameters describing the EDE dynamics.

Appendix C: Results for the local and early interaction models

In this appendix, we provide all the necessary material for the *i*EDE early and *i*EDE local scenarios: the cosmological constraints are displayed in Tabs. III and IV, while the 2D posterior distributions reconstructed from the \mathcal{D} , \mathcal{DH} , \mathcal{DS} and \mathcal{DHS} datasets are displayed in Figs. 7 and 8.

Appendix D: χ^2 tables

In this appendix, we report the best-fit χ^2 per experiment for the Λ CDM model, the EDE model, as well as the three *i*EDE scenarios for several combinations of data.

-
- [1] Elcio Abdalla et al., ‘‘Cosmology intertwined: A review of the particle physics, astrophysics, and cosmology associated with the cosmological tensions and anomalies,’’ *JHEAp* **34**, 49–211 (2022), arXiv:2203.06142 [astro-ph.CO].
- [2] Wendy L. Freedman, ‘‘Measurements of the Hubble Constant: Tensions in Perspective,’’ (2021), arXiv:2106.15656 [astro-ph.CO].
- [3] Adam G. Riess et al., ‘‘A Comprehensive Measurement of the Local Value of the Hubble Constant with 1 km/s/Mpc Uncertainty from the Hubble Space Telescope and the SH0ES Team,’’ (2021), arXiv:2112.04510 [astro-ph.CO].
- [4] A. Amon et al., ‘‘Consistent lensing and clustering in a low- S_8 Universe with BOSS, DES Year 3, HSC Year 1 and KiDS-1000,’’ (2022), arXiv:2202.07440 [astro-ph.CO].

EDE				
	\mathcal{D}	\mathcal{DH}	\mathcal{DS}	\mathcal{DHS}
$f_{\text{EDE}}(z_c)$	$< 0.037(0.016)$	$0.063(0.069) \pm 0.013$	$< 0.022(0.007)$	$0.045(0.050) \pm 0.012$
$\log_{10}(z_c)$	unconstrained(3.96)	$3.784(3.828) \pm 0.076$	unconstrained(3.98)	$3.79(3.88)^{+0.20}_{-0.17}$
Θ_i	unconstrained(3.08)	$> 1.52(2.87)$	unconstrained(3.04)	$> 1.37(2.93)$
H_0	$68.34(68.45)^{+0.48}_{-0.86}$	$71.43(71.69) \pm 0.74$	$68.61(68.51)^{+0.36}_{-0.56}$	$71.19(71.29) \pm 0.74$
ω_{cdm}	$0.1215(0.1223)^{+0.0011}_{-0.0025}$	$0.1298(0.1311) \pm 0.0030$	$0.1191(0.1191)^{+0.0008}_{-0.0015}$	$0.1247(0.1257) \pm 0.0024$
$10^2 \omega_b$	$2.248(2.257)^{+0.016}_{-0.019}$	$2.291(2.295) \pm 0.019$	$2.252(2.253) \pm 0.016$	$2.292(2.298) \pm 0.019$
$10^9 A_s$	$2.111(2.105)^{+0.027}_{-0.032}$	$2.142(2.148)^{+0.029}_{-0.033}$	$2.084(2.083)^{+0.024}_{-0.030}$	$2.110(2.108)^{+0.027}_{-0.030}$
n_s	$0.9683(0.9701)^{+0.0042}_{-0.0063}$	$0.9880(0.9907) \pm 0.0060$	$0.9687(0.9687)^{+0.0040}_{-0.0045}$	$0.9849(0.9866) \pm 0.0058$
τ_{reio}	$0.0566(0.0548)^{+0.0064}_{-0.0074}$	$0.0587(0.0595)^{+0.0068}_{-0.0076}$	$0.0533(0.0529)^{+0.0056}_{-0.0073}$	$0.0560(0.0562) \pm 0.0069$
S_8	$0.827(0.829) \pm 0.010$	$0.835(0.839) \pm 0.012$	$0.8054(0.807) \pm 0.0078$	$0.8067(0.810) \pm 0.0085$
Ω_m	$0.3097(0.3105) \pm 0.0052$	$0.3006(0.3009) \pm 0.0048$	$0.3022(0.3032) \pm 0.0043$	$0.2926(0.2938) \pm 0.0041$

TABLE III. Mean (best-fit) $\pm 1\sigma$ (or 2σ for one-sided bounds) of reconstructed parameters of the regular EDE model confronted to various datasets.

iEDE early				
	\mathcal{D}	\mathcal{DH}	\mathcal{DS}	\mathcal{DHS}
$f_{\text{EDE}}(z_c)$	$< 0.033(0.010)$	$0.064(0.070) \pm 0.014$	$< 0.030(0.001)$	$0.050(0.059) \pm 0.012$
$\log_{10}(z_c)$	unconstrained(3.755)	$3.765(3.822)^{+0.063}_{-0.082}$	$> 3.280(3.985)$	$3.783(3.809)^{+0.054}_{-0.073}$
Θ_i	unconstrained(0.45)	$> 1.17(2.86)$	unconstrained(0.19)	$> 0.84(2.84)$
$\log_{10}[\Gamma/a_c H_c]$	$< 0.2(-0.81)$	$< -0.6(-2.18)$	$-0.73(0.95)^{+1.60}_{-0.64}$	$-1.07(-0.60)^{+0.69}_{-0.10}$
H_0	$68.24(68.07)^{+0.43}_{-0.81}$	$71.44(71.82) \pm 0.80$	$68.46(67.89)^{+0.46}_{-0.80}$	$71.19(71.67) \pm 0.71$
ω_{idm}	$0.1213(0.1216)^{+0.0012}_{-0.0025}$	$0.1303(0.1311) \pm 0.0031$	$0.1202(0.1194)^{+0.0011}_{-0.0022}$	$0.1268(0.1289)^{+0.0026}_{-0.0030}$
$10^2 \omega_b$	$2.248(2.254)^{+0.017}_{-0.020}$	$2.295(2.298) \pm 0.020$	$2.258(2.251)^{+0.018}_{-0.022}$	$2.304(2.311) \pm 0.018$
$10^9 A_s$	$2.112(2.114)^{+0.028}_{-0.034}$	$2.148(2.145) \pm 0.032$	$2.099(2.101)^{+0.027}_{-0.034}$	$2.130(2.144)^{+0.028}_{-0.034}$
n_s	$0.9685(0.9691)^{+0.0043}_{-0.0063}$	$0.9886(0.9915) \pm 0.0063$	$0.9714(0.9691)^{+0.0048}_{-0.0064}$	$0.9898(0.9969) \pm 0.0063$
τ_{reio}	$0.0567(0.0563)^{+0.0064}_{-0.0076}$	$0.0596(0.0597)^{+0.0065}_{-0.0080}$	$0.0544(0.0548)^{+0.0061}_{-0.0076}$	$0.0576(0.0591)^{+0.0065}_{-0.0075}$
S_8	$0.823(0.817)^{+0.012}_{-0.011}$	$0.832(0.836)^{+0.013}_{-0.011}$	$0.795(0.784)^{+0.012}_{-0.010}$	$0.8001(0.7976) \pm 0.0099$
Ω_m	$0.3102(0.3125) \pm 0.0054$	$0.3016(0.3000) \pm 0.0051$	$0.3062(0.3092) \pm 0.0056$	$0.2970(0.2971)^{+0.0042}_{-0.0050}$

iEDE local				
	\mathcal{D}	\mathcal{DH}	\mathcal{DS}	\mathcal{DHS}
$f_{\text{EDE}}(z_c)$	$< 0.037(0.021)$	$0.064(0.07)^{+0.014}_{-0.013}$	$< 0.020(2 \times 10^{-4})$	$0.046(0.050)^{+0.015}_{-0.012}$
$\log_{10}(z_c)$	$> 3.26(3.93)$	$3.789(3.846)^{+0.067}_{-0.084}$	unconstrained(3.43)	$> 3.65(3.86)$
Θ_i	unconstrained(3.09)	$> 1.06(2.90)$	unconstrained(1.14)	unconstrained(2.91)
$\log_{10}[\Gamma/a_c H_c]$	$< -2.38(-4.24)$	$< -2.63(-3.79)$	$< -0.30(-0.72)$	$< -2.47(-3.91)$
H_0	$68.34(68.81)^{+0.49}_{-0.85}$	$71.48(71.63)^{+0.80}_{-0.70}$	$68.07(67.60)^{+0.48}_{-0.79}$	$71.13(71.50) \pm 0.78$
ω_{idm}	$0.1216(0.1231)^{+0.0013}_{-0.0027}$	$0.1302(0.1311) \pm 0.0030$	$0.1194(0.1193)^{+0.0008}_{-0.0011}$	$0.1251(0.1263) \pm 0.0027$
$10^2 \omega_b$	$2.248(2.257) \pm 0.018$	$2.294(2.296)^{+0.020}_{-0.018}$	$2.241(2.232)^{+0.016}_{-0.019}$	$2.295(2.299) \pm 0.020$
$10^9 A_s$	$2.109(2.114) \pm 0.031$	$2.147(2.140)^{+0.028}_{-0.033}$	$2.097(2.108)^{+0.028}_{-0.033}$	$2.111(2.107)^{+0.027}_{-0.030}$
n_s	$0.9688(0.9731)^{+0.0044}_{-0.0065}$	$0.9886(0.9905)^{+0.0065}_{-0.0057}$	$0.9668(0.9645)^{+0.0036}_{-0.0052}$	$0.9853(0.9883)^{+0.0066}_{-0.0059}$
τ_{reio}	$0.0562(0.0561) \pm 0.0069$	$0.0602(0.0584)^{+0.0063}_{-0.0079}$	$0.0555(0.0577)^{+0.0067}_{-0.0080}$	$0.0561(0.0551) \pm 0.0068$
S_8	$0.825(0.831) \pm 0.011$	$0.835(0.838) \pm 0.011$	$0.795(0.785)^{+0.016}_{-0.012}$	$0.8067(0.810) \pm 0.0086$
Ω_m	$0.3099(0.3090) \pm 0.0053$	$0.3009(0.3015) \pm 0.0045$	$0.3076(0.3114) \pm 0.0063$	$0.2939(0.2932) \pm 0.0044$

TABLE IV. Mean (best-fit) $\pm 1\sigma$ (or 2σ for one-sided bounds) of reconstructed parameters of the *i*EDE early and *i*EDE local models confronted to various datasets.

ph.CO].

- [5] Giovanni Aricò, Raul E. Angulo, Matteo Zennaro, Sergio Contreras, Angela Chen, and Carlos Hernández-Monteaquedo, “DES Y3 cosmic shear down to small scales: constraints on cosmology and baryons,” (2023), arXiv:2303.05537 [astro-ph.CO].
- [6] Tanvi Karwal and Marc Kamionkowski, “Dark energy at early times, the Hubble parameter, and the string axiverse,” Phys. Rev. **D94**, 103523 (2016), arXiv:1608.01309

[astro-ph.CO].

- [7] Vivian Poulin, Tristan L. Smith, Tanvi Karwal, and Marc Kamionkowski, “Early Dark Energy Can Resolve The Hubble Tension,” Phys. Rev. Lett. **122**, 221301 (2019), arXiv:1811.04083 [astro-ph.CO].
- [8] Tristan L. Smith, Vivian Poulin, and Mustafa A. Amin, “Oscillating scalar fields and the Hubble tension: a resolution with novel signatures,” Phys. Rev. D **101**, 063523 (2020), arXiv:1908.06995 [astro-ph.CO].

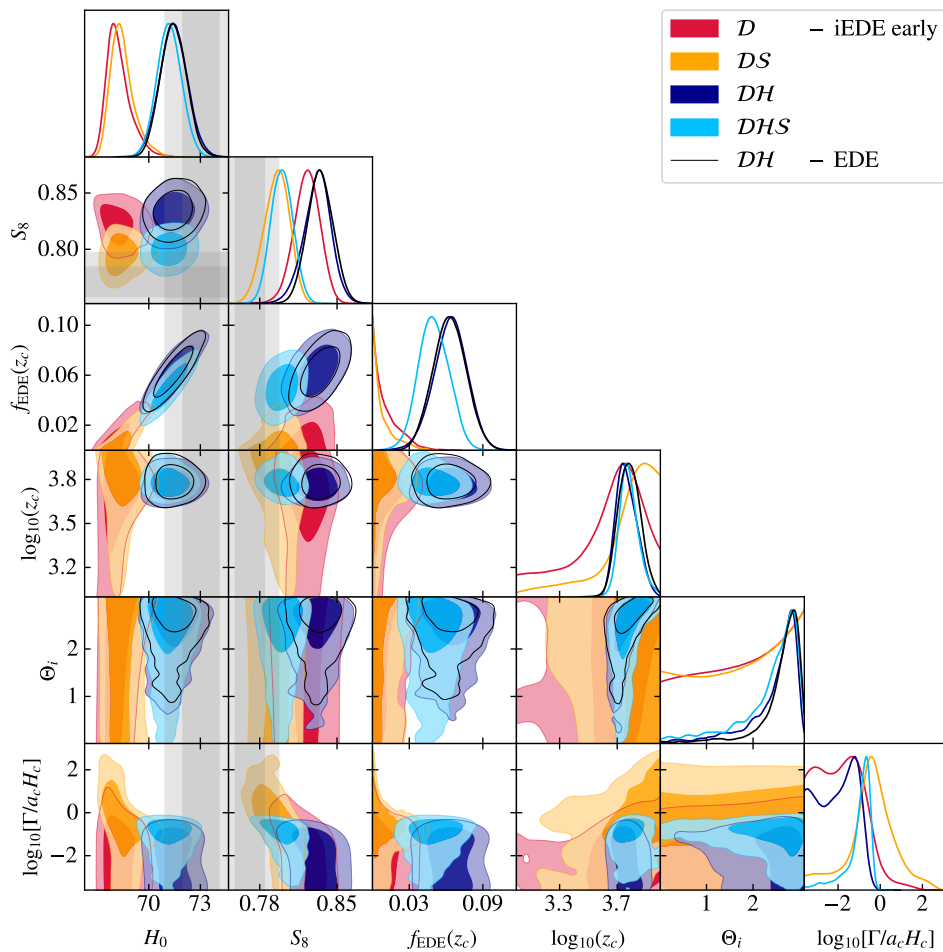


FIG. 7. 2D posterior distributions reconstructed from the \mathcal{D} , \mathcal{DH} , \mathcal{DS} and \mathcal{DHS} datasets for the early-interaction EDE scenario. For comparison, we also display the standard EDE 2D posterior distributions reconstructed from the \mathcal{DH} dataset. The gray bands show the H_0 and S_8 priors defined in Sec. III.

- [9] Vivian Poulin, Tristan L. Smith, and Tanvi Karwal, “The Ups and Downs of Early Dark Energy solutions to the Hubble tension: a review of models, hints and constraints circa 2023,” (2023), arXiv:2302.09032 [astro-ph.CO].
- [10] Eleonora Di Valentino, Olga Mena, Supriya Pan, Luca Visinelli, Weiqiang Yang, Alessandro Melchiorri, David F. Mota, Adam G. Riess, and Joseph Silk, “In the realm of the Hubble tension—a review of solutions,” *Class. Quant. Grav.* **38**, 153001 (2021), arXiv:2103.01183 [astro-ph.CO].
- [11] Nils Schöneberg, Guillermo Franco Abellán, Andrea Pérez Sánchez, Samuel J. Witte, Vivian Poulin, and Julien Lesgourgues, “The H_0 Olympics: A fair ranking of proposed models,” (2021), arXiv:2107.10291 [astro-ph.CO].
- [12] Karsten Jedamzik and Levon Pogosian, “Relieving the Hubble tension with primordial magnetic fields,” (2020), arXiv:2004.09487 [astro-ph.CO].
- [13] Vivian Poulin, Tristan L. Smith, Rodrigo Calderón, and Théo Simon, “On the implications of the ‘cosmic calibration tension’ beyond H_0 and the synergy between early- and late-time new physics,” (2024), arXiv:2407.18292 [astro-ph.CO].
- [14] J. Colin Hill, Evan McDonough, Michael W. Toomey, and Stephon Alexander, “Early dark energy does not restore cosmological concordance,” *Phys. Rev. D* **102**, 043507 (2020), arXiv:2003.07355 [astro-ph.CO].
- [15] Riccardo Murgia, Guillermo F. Abellán, and Vivian Poulin, “Early dark energy resolution to the Hubble tension in light of weak lensing surveys and lensing anomalies,” *Phys. Rev. D* **103**, 063502 (2021), arXiv:2009.10733 [astro-ph.CO].
- [16] Julien Lesgourgues, Gustavo Marques-Tavares, and Martin Schmaltz, “Evidence for dark matter interactions in cosmological precision data?” *JCAP* **02**, 037 (2016), arXiv:1507.04351 [astro-ph.CO].
- [17] Manuel A. Buen-Abad, Gustavo Marques-Tavares, and Martin Schmaltz, “Non-Abelian dark matter and dark radiation,” *Phys. Rev. D* **92**, 023531 (2015), arXiv:1505.03542 [hep-ph].
- [18] Zackaria Chacko, Yanou Cui, Sungwoo Hong, Takemichi Okui, and Yuhsin Tsai, “Partially Acoustic Dark Matter, Interacting Dark Radiation, and Large Scale Structure,”

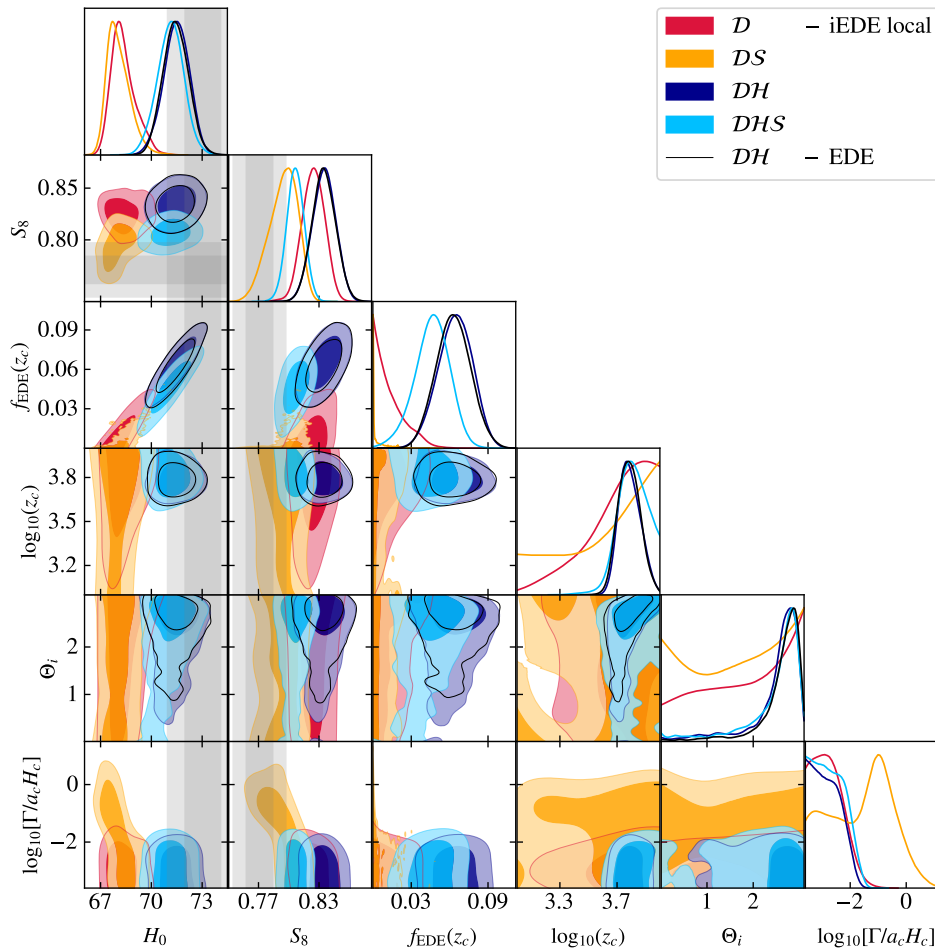


FIG. 8. 2D posterior distributions reconstructed from the \mathcal{D} , \mathcal{DH} , \mathcal{DS} and \mathcal{DHS} datasets for the local-interaction EDE scenario. For comparison, we also display the standard EDE 2D posterior distributions reconstructed from the \mathcal{DH} dataset. The gray bands show the H_0 and S_8 priors defined in Sec. III.

- JHEP **12**, 108 (2016), arXiv:1609.03569 [astro-ph.CO].
- [19] Manuel A. Buen-Abad, Martin Schmaltz, Julien Lesgourgues, and Thejs Brinckmann, “Interacting Dark Sector and Precision Cosmology,” JCAP **01**, 008 (2018), arXiv:1708.09406 [astro-ph.CO].
- [20] Stefan Heimersheim, Nils Schöneberg, Deanna C. Hooper, and Julien Lesgourgues, “Cannibalism hinders growth: Cannibal Dark Matter and the S_8 tension,” JCAP **12**, 016 (2020), arXiv:2008.08486 [astro-ph.CO].
- [21] Eleonora Di Valentino, Alessandro Melchiorri, Olga Mena, and Sunny Vagnozzi, “Interacting dark energy in the early 2020s: A promising solution to the H_0 and cosmic shear tensions,” Phys. Dark Univ. **30**, 100666 (2020), arXiv:1908.04281 [astro-ph.CO].
- [22] Matteo Lucca, “Dark energy–dark matter interactions as a solution to the S_8 tension,” (2021), arXiv:2105.09249 [astro-ph.CO].
- [23] Guillermo F. Abellan, Riccardo Murgia, Vivian Poulin, and Julien Lavalle, “Hints for decaying dark matter from S_8 measurements,” (2020), arXiv:2008.09615 [astro-ph.CO].
- [24] Eleonora Di Valentino et al., “Cosmology Intertwined III: $f\sigma_8$ and S_8 ,” Astropart. Phys. **131**, 102604 (2021), arXiv:2008.11285 [astro-ph.CO].
- [25] Saurabh Bansal, Jeong Han Kim, Christopher Kolda, Matthew Low, and Yuhsin Tsai, “Mirror twin Higgs cosmology: constraints and a possible resolution to the H_0 and S_8 tensions,” JHEP **05**, 050 (2022), arXiv:2110.04317 [hep-ph].
- [26] Marco Baldi and Fergus Simpson, “Structure formation simulations with momentum exchange: alleviating tensions between high-redshift and low-redshift cosmological probes,” Mon. Not. Roy. Astron. Soc. **465**, 653–666 (2017), arXiv:1605.05623 [astro-ph.CO].
- [27] Suresh Kumar and Rafael C. Nunes, “Observational constraints on dark matter–dark energy scattering cross section,” Eur. Phys. J. C **77**, 734 (2017), arXiv:1709.02384 [astro-ph.CO].
- [28] Mahnaz Asghari, Jose Beltrán Jiménez, Shahram Khosravi, and David F. Mota, “On structure formation from a small-scales-interacting dark sector,” JCAP **04**, 042 (2019), arXiv:1902.05532 [astro-ph.CO].

Data	Model	χ^2 tot	P18TTTEE	P18lens	ext-BAO	BOSS	eBOSS	Pan+	M_b	S_8
\mathcal{D}	Λ CDM	4405.00	2762.10	8.86	1.22	160.27	61.20	1411.35	–	–
	EDE	4401.85	2759.08	9.06	1.22	160.72	60.37	1411.39	–	–
	iEDE early	4401.70	2759.18	9.02	1.30	160.29	60.36	1411.56	–	–
	iEDE local	4401.17	2758.28	9.14	1.28	160.60	60.32	1411.55	–	–
	iEDE late	4401.30	2758.75	9.06	1.29	160.31	60.35	1411.54	–	–
\mathcal{DH}	Λ CDM	4442.48	2766.43	9.47	2.06	158.03	60.50	1413.34	32.65	–
	EDE	4412.38	2762.30	9.84	1.85	160.42	60.54	1413.09	4.35	–
	iEDE early	4412.34	2762.59	9.87	1.93	160.30	60.57	1413.27	3.81	–
	iEDE local	4412.34	2762.15	9.87	1.88	160.33	60.51	1413.15	4.45	–
	iEDE late	4412.16	2763.02	9.93	1.79	159.91	60.71	1412.93	3.82	–
\mathcal{DS}	Λ CDM	4414.79	2764.32	10.38	1.85	158.22	60.74	1412.85	–	6.43
	EDE	4414.14	2762.47	10.43	1.74	158.45	60.71	1412.62	–	7.71
	iEDE early	4409.89	2763.59	9.57	1.27	161.87	61.18	1411.47	–	0.95
	iEDE local	4409.95	2763.89	9.47	1.19	161.06	61.93	1411.26	–	1.15
	iEDE late	4404.18	2759.20	9.29	1.35	161.30	60.83	1411.73	–	0.48
\mathcal{DHS}	Λ CDM	4447.50	2768.46	10.86	2.52	158.16	60.77	1414.39	28.96	3.38
	EDE	4427.87	2763.99	11.27	2.59	158.82	60.53	1414.76	6.91	8.99
	iEDE early	4423.10	2768.14	10.68	2.24	158.31	61.05	1413.95	4.63	4.11
	iEDE local	4427.73	2764.54	11.54	2.71	159.06	60.58	1415.02	5.36	8.91
	iEDE late	4413.59	2764.26	9.85	1.80	159.98	60.82	1412.96	3.60	0.32

TABLE V. Best-fit χ^2 of the different models considered in this work (Λ CDM, EDE and iEDE) for various combinations of likelihood.

- [29] Jose Beltrán Jiménez, Dario Bettoni, David Figueruelo, Florencia A. Teppa Pannia, and Shinji Tsujikawa, “Velocity-dependent interacting dark energy and dark matter with a Lagrangian description of perfect fluids,” *JCAP* **03**, 085 (2021), arXiv:2012.12204 [astro-ph.CO].
- [30] David Figueruelo et al., “J-PAS: Forecasts for dark matter - dark energy elastic couplings,” *JCAP* **07**, 022 (2021), arXiv:2103.01571 [astro-ph.CO].
- [31] Jose Beltrán Jiménez, Dario Bettoni, David Figueruelo, Florencia Anabella Teppa Pannia, and Shinji Tsujikawa, “Probing elastic interactions in the dark sector and the role of S_8 ,” *Phys. Rev. D* **104**, 103503 (2021), arXiv:2106.11222 [astro-ph.CO].
- [32] Vivian Poulin, José Luis Bernal, Ely Kovetz, and Marc Kamionkowski, “The Sigma-8 Tension is a Drag,” (2022), arXiv:2209.06217 [astro-ph.CO].
- [33] Alexandra Amon and George Efstathiou, “A non-linear solution to the S_8 tension?” (2022), arXiv:2206.11794 [astro-ph.CO].
- [34] Clément Stahl, Benoit Famaey, Rodrigo Ibata, Oliver Hahn, Nicolas Martinet, and Thomas Montandon, “Scale-dependent local primordial non-Gaussianity as a solution to the S_8 tension,” (2024), arXiv:2404.03244 [astro-ph.CO].
- [35] Alkistis Pourtsidou and Thomas Tram, “Reconciling CMB and structure growth measurements with dark energy interactions,” *Phys. Rev. D* **94**, 043518 (2016), arXiv:1604.04222 [astro-ph.CO].
- [36] Evan McDonough, Meng-Xiang Lin, J. Colin Hill, Wayne Hu, and Shengjia Zhou, “Early dark sector, the Hubble tension, and the swampland,” *Phys. Rev. D* **106**, 043525 (2022), arXiv:2112.09128 [astro-ph.CO].
- [37] Tanvi Karwal, Marco Raveri, Bhuvnesh Jain, Justin Khoury, and Mark Trodden, “Chameleon Early Dark Energy and the Hubble Tension,” (2021), arXiv:2106.13290 [astro-ph.CO].
- [38] Gang Liu, Jiaze Gao, Yufen Han, Yuhao Mu, and Lixin Xu, “Mitigating Cosmological Tensions via Momentum-Coupled Dark Sector Model,” (2023), arXiv:2310.09798 [astro-ph.CO].
- [39] Gang Liu, Yuhao Mu, Jiaze Gao, Yufen Han, and Lixin Xu, “The Yukawa-Coupled Dark Sector Model and Cosmological Tensions,” (2023), arXiv:2312.01410 [astro-ph.CO].
- [40] Gang Liu, Zhihuan Zhou, Yuhao Mu, and Lixin Xu, “Kinetically coupled scalar fields model and cosmological tensions,” *Mon. Not. Roy. Astron. Soc.* **529**, 1852–1861 (2024), arXiv:2308.07069 [astro-ph.CO].
- [41] Gabriela Garcia-Arroyo, L. Arturo Ureña López, and J. Alberto Vázquez, “Interacting Scalar fields: Dark Matter–Early Dark Energy,” (2024), arXiv:2402.08815 [astro-ph.CO].
- [42] A. Pourtsidou, C. Skordis, and E. J. Copeland, “Models of dark matter coupled to dark energy,” *Phys. Rev. D* **88**, 083505 (2013), arXiv:1307.0458 [astro-ph.CO].
- [43] Rachel Bean, Eanna E. Flanagan, Istvan Laszlo, and Mark Trodden, “Constraining Interactions in Cosmology’s Dark Sector,” *Phys. Rev. D* **78**, 123514 (2008), arXiv:0808.1105 [astro-ph].
- [44] Stéphane Ilić, Michael Kopp, Constantinos Skordis, and Daniel B. Thomas, “Dark matter properties through cosmic history,” *Phys. Rev. D* **104**, 043520 (2021), arXiv:2004.09572 [astro-ph.CO].
- [45] Chung-Pei Ma and Edmund Bertschinger, “Cosmological perturbation theory in the synchronous and conformal Newtonian gauges,” *Astrophys. J.* **455**, 7–25 (1995), arXiv:astro-ph/9506072.
- [46] Vivian Poulin, Tristan L. Smith, Daniel Grin, Tanvi Karwal, and Marc Kamionkowski, “Cosmological implications of ultralight axionlike fields,” *Phys. Rev. D* **98**, 083525 (2018), arXiv:1806.10608 [astro-ph.CO].

- [47] J. Colin Hill *et al.*, “The Atacama Cosmology Telescope: Constraints on Pre-Recombination Early Dark Energy,” (2021), arXiv:2109.04451 [astro-ph.CO].
- [48] Vivian Poulin, Tristan L. Smith, and Alexa Bartlett, “Dark Energy at early times and ACT: a larger Hubble constant without late-time priors,” (2021), arXiv:2109.06229 [astro-ph.CO].
- [49] George Efstathiou, Erik Rosenberg, and Vivian Poulin, “Improved Planck constraints on axion-like early dark energy as a resolution of the Hubble tension,” (2023), arXiv:2311.00524 [astro-ph.CO].
- [50] Meng-Xiang Lin, Giampaolo Benevento, Wayne Hu, and Marco Raveri, “Acoustic Dark Energy: Potential Conversion of the Hubble Tension,” *Phys. Rev. D* **100**, 063542 (2019), arXiv:1905.12618 [astro-ph.CO].
- [51] Florian Niedermann and Martin S. Sloth, “New Early Dark Energy,” (2019), arXiv:1910.10739 [astro-ph.CO].
- [52] Fergus Simpson, “Scattering of dark matter and dark energy,” *Phys. Rev. D* **82**, 083505 (2010), arXiv:1007.1034 [astro-ph.CO].
- [53] Melissa Joseph, Daniel Aloni, Martin Schmaltz, Eashwar N. Sivarajan, and Neal Weiner, “A Step in understanding the S8 tension,” *Phys. Rev. D* **108**, 023520 (2023), arXiv:2207.03500 [astro-ph.CO].
- [54] Thejs Brinckmann and Julien Lesgourgues, “MontePython 3: boosted MCMC sampler and other features,” (2018), arXiv:1804.07261 [astro-ph.CO].
- [55] Benjamin Audren, Julien Lesgourgues, Karim Benabed, and Simon Prunet, “Conservative Constraints on Early Cosmology: an illustration of the Monte Python cosmological parameter inference code,” *JCAP* **1302**, 001 (2013), arXiv:1210.7183 [astro-ph.CO].
- [56] Julien Lesgourgues, “The Cosmic Linear Anisotropy Solving System (CLASS) I: Overview,” (2011), arXiv:1104.2932 [astro-ph.IM].
- [57] Diego Blas, Julien Lesgourgues, and Thomas Tram, “The Cosmic Linear Anisotropy Solving System (CLASS) II: Approximation schemes,” *JCAP* **1107**, 034 (2011), arXiv:1104.2933 [astro-ph.CO].
- [58] N. Aghanim *et al.* (Planck), “Planck 2018 results. V. CMB power spectra and likelihoods,” *Astron. Astrophys.* **641**, A5 (2020), arXiv:1907.12875 [astro-ph.CO].
- [59] N. Aghanim *et al.* (Planck), “Planck 2018 results. VIII. Gravitational lensing,” *Astron. Astrophys.* **641**, A8 (2020), arXiv:1807.06210 [astro-ph.CO].
- [60] Florian Beutler, Chris Blake, Matthew Colless, D. Heath Jones, Lister Staveley-Smith, Lachlan Campbell, Quentin Parker, Will Saunders, and Fred Watson, “The 6dF Galaxy Survey: Baryon Acoustic Oscillations and the Local Hubble Constant,” *Mon. Not. Roy. Astron. Soc.* **416**, 3017–3032 (2011), arXiv:1106.3366 [astro-ph.CO].
- [61] Ashley J. Ross, Lado Samushia, Cullan Howlett, Will J. Percival, Angela Burden, and Marc Manera, “The clustering of the SDSS DR7 main Galaxy sample – I. A 4 per cent distance measure at $z = 0.15$,” *Mon. Not. Roy. Astron. Soc.* **449**, 835–847 (2015), arXiv:1409.3242 [astro-ph.CO].
- [62] Héctor Gil-Marín *et al.*, “The clustering of galaxies in the SDSS-III Baryon Oscillation Spectroscopic Survey: BAO measurement from the LOS-dependent power spectrum of DR12 BOSS galaxies,” *Mon. Not. Roy. Astron. Soc.* **460**, 4210–4219 (2016), arXiv:1509.06373 [astro-ph.CO].
- [63] Shadab Alam *et al.* (BOSS), “The clustering of galaxies in the completed SDSS-III Baryon Oscillation Spectroscopic Survey: cosmological analysis of the DR12 galaxy sample,” *Mon. Not. Roy. Astron. Soc.* **470**, 2617–2652 (2017), arXiv:1607.03155 [astro-ph.CO].
- [64] Francisco-Shu Kitaura *et al.*, “The clustering of galaxies in the SDSS-III Baryon Oscillation Spectroscopic Survey: mock galaxy catalogues for the BOSS Final Data Release,” *Mon. Not. Roy. Astron. Soc.* **456**, 4156–4173 (2016), arXiv:1509.06400 [astro-ph.CO].
- [65] Pierre Zhang, Guido D’Amico, Leonardo Senatore, Cheng Zhao, and Yifu Cai, “BOSS Correlation Function analysis from the Effective Field Theory of Large-Scale Structure,” *JCAP* **02**, 036 (2022), arXiv:2110.07539 [astro-ph.CO].
- [66] Beth Reid *et al.*, “SDSS-III Baryon Oscillation Spectroscopic Survey Data Release 12: galaxy target selection and large scale structure catalogues,” *Mon. Not. Roy. Astron. Soc.* **455**, 1553–1573 (2016), arXiv:1509.06529 [astro-ph.CO].
- [67] Guido D’Amico, Leonardo Senatore, and Pierre Zhang, “Limits on w CDM from the EFTofLSS with the PyBird code,” (2020), arXiv:2003.07956 [astro-ph.CO].
- [68] José Luis Bernal, Tristan L. Smith, Kimberly K. Boddy, and Marc Kamionkowski, “Robustness of baryon acoustic oscillations constraints to beyond- Λ CDM cosmologies,” (2020), arXiv:2004.07263 [astro-ph.CO].
- [69] Guido D’Amico, Leonardo Senatore, Pierre Zhang, and Henry Zheng, “The Hubble Tension in Light of the Full-Shape Analysis of Large-Scale Structure Data,” (2020), arXiv:2006.12420 [astro-ph.CO].
- [70] Tristan L. Smith, Vivian Poulin, José Luis Bernal, Kimberly K. Boddy, Marc Kamionkowski, and Riccardo Murgia, “Early dark energy is not excluded by current large-scale structure data,” *Phys. Rev. D* **103**, 123542 (2021), arXiv:2009.10740 [astro-ph.CO].
- [71] Mikhail M. Ivanov, Evan McDonough, J. Colin Hill, Marko Simonović, Michael W. Toomey, Stephon Alexander, and Matias Zaldarriaga, “Constraining Early Dark Energy with Large-Scale Structure,” *Phys. Rev. D* **102**, 103502 (2020), arXiv:2006.11235 [astro-ph.CO].
- [72] Théo Simon, Pierre Zhang, Vivian Poulin, and Tristan L. Smith, “Updated constraints from the effective field theory analysis of the BOSS power spectrum on early dark energy,” *Phys. Rev. D* **107**, 063505 (2023), arXiv:2208.05930 [astro-ph.CO].
- [73] Théo Simon, “Can acoustic and axionlike early dark energy still resolve the Hubble tension?” *Phys. Rev. D* **110**, 023528 (2024), arXiv:2310.16800 [astro-ph.CO].
- [74] Rafaela Gsponer, Ruiyang Zhao, Jamie Donald-McCann, David Bacon, Kazuya Koyama, Robert Crittenden, Theo Simon, and Eva-Maria Mueller, “Cosmological constraints on early dark energy from the full shape analysis of eBOSS DR16,” *Mon. Not. Roy. Astron. Soc.* **530**, 3075–3099 (2024), arXiv:2312.01977 [astro-ph.CO].
- [75] Théo Simon, Pierre Zhang, Vivian Poulin, and Tristan L. Smith, “On the consistency of effective field theory analyses of BOSS power spectrum,” (2022), arXiv:2208.05929 [astro-ph.CO].
- [76] Emil Brinch Holm, Laura Herold, Théo Simon, Elisa G. M. Ferreira, Steen Hannestad, Vivian Poulin, and Thomas Tram, “Bayesian and frequentist investigation of prior effects in EFT of LSS analyses of full-shape BOSS and eBOSS data,” *Phys. Rev. D* **108**, 123514 (2023),

- arXiv:2309.04468 [astro-ph.CO].
- [77] Théo Simon, Pierre Zhang, and Vivian Poulin, “Cosmological inference from the EFTofLSS: the eBOSS QSO full-shape analysis,” (2022), arXiv:2210.14931 [astro-ph.CO].
- [78] Shadab Alam *et al.* (eBOSS), “Completed SDSS-IV extended Baryon Oscillation Spectroscopic Survey: Cosmological implications from two decades of spectroscopic surveys at the Apache Point Observatory,” *Phys. Rev. D* **103**, 083533 (2021), arXiv:2007.08991 [astro-ph.CO].
- [79] Ashley J. Ross *et al.*, “The Completed SDSS-IV extended Baryon Oscillation Spectroscopic Survey: Large-scale structure catalogues for cosmological analysis,” *Mon. Not. Roy. Astron. Soc.* **498**, 2354–2371 (2020), arXiv:2007.09000 [astro-ph.CO].
- [80] Chia-Hsun Chuang, Francisco-Shu Kitaura, Francisco Prada, Cheng Zhao, and Gustavo Yepes, “EZmocks: extending the Zel’dovich approximation to generate mock galaxy catalogues with accurate clustering statistics,” *Mon. Not. Roy. Astron. Soc.* **446**, 2621–2628 (2015), arXiv:1409.1124 [astro-ph.CO].
- [81] Florian Beutler and Patrick McDonald, “Unified galaxy power spectrum measurements from 6dFGS, BOSS, and eBOSS,” *JCAP* **11**, 031 (2021), arXiv:2106.06324 [astro-ph.CO].
- [82] Jiamin Hou *et al.*, “The Completed SDSS-IV extended Baryon Oscillation Spectroscopic Survey: BAO and RSD measurements from anisotropic clustering analysis of the Quasar Sample in configuration space between redshift 0.8 and 2.2,” *Mon. Not. Roy. Astron. Soc.* **500**, 1201–1221 (2020), arXiv:2007.08998 [astro-ph.CO].
- [83] Dillon Brout *et al.*, “The Pantheon+ Analysis: Cosmological Constraints,” (2022), arXiv:2202.04077 [astro-ph.CO].
- [84] Catherine Heymans *et al.*, “KiDS-1000 Cosmology: Multi-probe weak gravitational lensing and spectroscopic galaxy clustering constraints,” *Astron. Astrophys.* **646**, A140 (2021), arXiv:2007.15632 [astro-ph.CO].
- [85] T. M. C. Abbott *et al.* (DES), “Dark Energy Survey Year 3 Results: Cosmological Constraints from Galaxy Clustering and Weak Lensing,” (2021), arXiv:2105.13549 [astro-ph.CO].
- [86] N. Aghanim *et al.* (Planck), “Planck 2018 results. VI. Cosmological parameters,” *Astron. Astrophys.* **641**, A6 (2020), [Erratum: *Astron. Astrophys.* 652, C4 (2021)], arXiv:1807.06209 [astro-ph.CO].
- [87] Antony Lewis, “GetDist: a Python package for analysing Monte Carlo samples,” (2019), arXiv:1910.13970 [astro-ph.IM].
- [88] Itamar J. Allali, Fabrizio Rompineve, and Mark P. Hertzberg, “Dark sectors with mass thresholds face cosmological datasets,” *Phys. Rev. D* **108**, 023527 (2023), arXiv:2305.14166 [astro-ph.CO].
- [89] Manuel A. Buen-Abad, Zackaria Chacko, Can Kilic, Gustavo Marques-Tavares, and Taewook Youn, “Stepped partially acoustic dark matter: likelihood analysis and cosmological tensions,” *JCAP* **11**, 005 (2023), arXiv:2306.01844 [astro-ph.CO].
- [90] Nils Schöneberg, Guillermo Franco Abellán, Théo Simon, Alexa Bartlett, Yashvi Patel, and Tristan L. Smith, “Comparative analysis of interacting stepped dark radiation,” *Phys. Rev. D* **108**, 123513 (2023), arXiv:2306.12469 [astro-ph.CO].
- [91] Matthew C. Johnson and Marc Kamionkowski, “Dynamical and Gravitational Instability of Oscillating-Field Dark Energy and Dark Matter,” *Phys. Rev. D* **78**, 063010 (2008), arXiv:0805.1748 [astro-ph].